PCCP

Accepted Manuscript

ROYAL SOCIETY OF CHEMISTRY

www.rsc.org/pccp

Perspective PCCP

How molecular is the chemisorptive bond?

R. A. v. Santen, I. Tranca

For E. J. Baerends on behalf of his 70th birthday

Abstract

Trends in adsorption energies as a function of transition metal differ for adsorbates that are attached atop of a surface atom or are adsorbed in a high coordination site. When adsorption to early and late transition metals is compared variation in relative bond energies of adsorbates attached to different sites is large. A theoretical understanding is provided based on the analysis of the electronic structure of the respective chemical bonds.

The electronic structure analysis is based on Partial Density of States (PDOS) and bond order overlap population densities from Crystal Orbital Hamiltonian Population (COHP) calculations available from DFT electronic structure computations. This is complemented with calculations of Bader charge densities and electron density topology properties.

Variation of respective bond energies depends on the symmetry of the molecular orbitals that form the chemical bond. Key electronic structure parameters are the position of the Fermi level in the bonding or antibonding molecular orbital partial density of state region of the chemical bond and chemical bond polarity. These are very different for adsorbates adsorbed to the same transition metal surface, but which have different coordination with surface metal atoms.

The adsorption energies and the respective electronic structures of ad atoms H, C and O and molecular fragments CH_x (x=1-3) are compared with those of the analogous molecules that contain a single transition metal atom. When adsorbed atop, trends in bond energies are remarkably similar to those of the corresponding molecules.

The difference in bond energies of adsorbates and transition metal molecules, i.e. the embedding energy, is shown to consist of three contributions: quenching of the sometimes high molecular spin states and weakening of the molecular and metal-metal atom bond energies next to the adsorbate.

Conventional scaling rules of the interaction energies of adsorbed CH_x ($0<x\leq3$) fragments are only satisfied for adsorbates in high coordination sites. For the early transition metals a breaking of this rule is found for C and CH or N and NH when adsorbed atop of a transition metal surface or when they are part of a transition metal molecule. The M-C bond energy is found to be only stronger than that of M-CH bond as long as the Fermi level or HOMO is located in the antibonding molecular orbital partial density of states of the chemical bond.

I. Introduction

There is a significant understanding of the electronic structure of the chemical bond [1–8] of adsorbates on transition metal surfaces. Detailed comparison of experimental spectroscopic data [9–13] and DFT calculations of electronic chemical bonding details demonstrate this through sometimes

impressive agreement [14, 15]. Such studies have been mainly concerned with adsorption to the late transition metals.

In this paper we will analyze trends in bond energies as a function of transition metal for adsorption on different sites. Especially when we include comparison between early and late transition metals bond energy trends show important differences compared to expectations based on studies of adsorption to the late transition metals only. We will analyze the electronic cause of these differences and discuss implications to the prediction of surface reactivity. For instance ,on the early transition metals scaling rules between bond energies of adsorbates and their component ad atoms are modified compared to classical scaling rule behavior on the late transition metals[16].

One of the first comprehensive papers on the transition metal surface reactivity based on DFT computed chemisorption data with periodic surface models is the Nørskov-Hammer paper [17]. As is also well described in [1] trends in adsorption energies of atoms and molecules adsorbed to the late transition metals can be understood based on varying distribution of valence electrons over the bonding and antibonding molecular orbital electron energy levels, that are formed by the interaction of adsorbate orbitals mainly with the transition metal d-valence electron band orbitals. On late transition metals the Fermi level tends to be located in the antibonding molecular orbital partial density of states, so that the adsorption energy is predicted to increase when transition metal valence electron band occupation decreases.

This indicates that transition metal valence band electron occupation is to be considered an important surface reactivity indicator [1, 13].It is related to ξ_d that is defined as the average energy of the transition metal d -valence electron energy band, with respect to the Fermi level, the highest electron occupied orbital energy Within the rigid band assumption that assumes that electronic structure does not change with transition metal but only valence electron occupation, ξ_d is a measure of the electron occupation of the transition metal valence electron band. Therefore it is widely used as a reactivity performance indicator since it is easily accessible from computations or measurements [1].

We will see that due to increased polarity of the adsorbate chemical bond for adsorbates attached to the surface of the early transition metals, ionic energy contributions to their bond energy become increasingly more important. This will modify bond energy trend predictions based on the rigid band assumption and the use of ξ_d as solely reactivity performance indicator.

We will compare here variation in adsorption energy as a function of ad atom coordination number. Atop and three fold coordinated adsorbates will be discussed. An important result is that the adsorption energy ratio between atop and threefold coordinated adsorbates, that we study here, is not a constant but varies with transition metal. This ratio is found to approximately vary between one and a halve

We will see that the symmetries of the molecular orbitals that form the adsorbate –surface bond are important electronic structure parameters. Important is also whether the Fermi level is located in the bonding or antibonding part of the molecular orbital partial density of states. The relative position of the Fermi level to the energy of the nonbonding molecular orbital partial density of states, that separates the two parts, varies largely at different adsorption sites.

Comparison of trends of the interaction energies of adsorbates as CH_x, NH_x or OH_x as a function of x have led to the identification of scaling rules that relate the adsorption energies of the XH_x fragments to the adsorption energy of free X atoms, [16, 18, 19] Generally it is found [18] that the bond energies decrease with increasing value of x.

Such scaling rules are highly useful to predict trends in reactivity of heterogeneous catalytic reactions. This is usually done through the application of Brønsted-Evans Polanyi (BEP) linear activation energy -reaction energy relations [20–22] that use the scaling rules to deduce energies of adsorption of surface fragments from that of the corresponding ad atoms.

Interestingly for the early transition metals a deviation from conventional scaling rule behavior is found. We will show that for the atop adsorbed atoms the bond energy of the C ad atom becomes less than that of CH adsorbate instead of the commonly higher value of the C ad atom bond energy. This happens for the surface chemical bonds when by a lower transition metal valence electron occupation the Fermi level changes from its position in the antibonding molecular orbital partial density of states to the bonding molecular orbital partial density of states.

Early work by Hoffmann [23, 24], originally based on semi-empirical electronic structure theory, provides theoretical guidance to the interpretation of the electronic structure of adsorbates. He defined as useful electronic structure functions the Partial Density of States (PDOS) and the Bond Order Overlap Population (BOOP) density, that can now be calculated from more accurate first principle DFT data [25–27]. An early application of the use of these DFT calculated electronic functions to the analysis of surface reactivity of Ag can be found in[28].

We will analyze the electronic structure of the surface chemical bond based on the calculated PDOS of the respective valence atomic orbitals of adsorbate and surface metal atoms and on the Crystal Orbital Hamiltonian Population Densities (COHP) which are a measure of the Bond Order Overlap Population density that recently have become available [25] for DFT calculations using the VASP code [29–32]. To analyze polarity of the chemical bond Bader charges and topological energy density properties [33–37] are calculated. Details of the methods and surface model used are given in section VII.

The integrated value of the PDOS is a measure of the atomic orbital electron occupation and the integrated value of the COHP is a measure of the covalent contribution to the surface chemical bond, respectively. The $COHP_{ij}$ (E) is proportional to the bond order overlap density at energy E weighted over the Hamilton matrix element H_{ij}, that is a measure of the interaction strength between atomic orbitals i and j. A negative versus positive sign of $COHP_{ij}$ (E) indicates bonding versus antibonding character of the molecular orbital density between atomic orbitals i and j. In order to associate the bonding nature of a molecular orbital or the molecular orbital partial density of states of a surface chemical bond to a positive sign we have plot in the figures that show bond order overlap population densities –COHP as a function of electron energy. . Its integrated value $ICOHP_{ij}$ is equal to the contribution to the bond energy of the interaction of atomic orbitals i and j, respectively, apart from a correction due to differences in electrostatic interactions [26].

The energy of the chemical bond is the sum of repulsive and attractive interactions. Within molecular orbital theory the repulsive interaction between adsorbate and surface atoms arises from the electron occupation of antibonding molecular orbital fragments and is called Pauli repulsion. The attractive interactions are due to the electron occupation of bonding molecular orbitals. Early implementation of such orbital analysis, as the energy decomposition analysis [38] based on DFT computations and applications to chemisorption can be found in[39–42].

In this paper based on state of the art DFT calculations we will analyze the electronic structure of the chemical bonds in terms of the distribution of electrons over bonding and antibonding molecular orbitals following the Baerends-Ziegler school.

Complementary to the ad atom surface bond we will also study analogous single transition metal molecules. By single transition metal atom molecule we understand herein any molecule formed from a single transition metal to which an atom or molecular fragment binds. Trends of bond energies and electronic structures are compared. There appears to be a remarkable parallel between trends in calculated molecular binding energies and those of atop adsorbed adsorbates. The potential of single transition metal atom as catalysts has recently become of interest [43–45]. Therefore reactivity data of transition metal molecules are of interest by itself.

For the hydride molecules Andrews et.al.[46] conclude that high quality DFT results compare well with correlated ab-initio calculations as MCSCF/MRCI. Comparison with experimental data on bond energies from Chen et.al.[47] indicates for VH and CrH that the DFT(PBE) calculated bond energies are too high by 30 kJ/mol, but show a similar bond energy difference. In this case CrH has the weaker bond.

Through the present paper we will use the same exchange-correlation functional (PBE) for both the molecular systems and the surfaces. This approach makes possible a systematic comparison of molecules and adsorbates.

Whereas the molecular orbital structure of a molecule is discrete in energy, the orbitals are distributed over continuous electron energy bands in the solids. This delocalization of the transition metal valence electrons has the important consequence that the bond strength of an adsorbate attached to a single surface atom compared to that of the related single transition metal atom molecule is lower.

In addition the broadening of the molecular energy levels of the ad atom-surface chemical bond will cause an overlap of the electron energies of molecular orbitals. Therefore hybridization is different on the surface than within the molecule.

An early important paper that compares the bonding in a molecule and to a surface is that of Siegbahn et.al.[48], who recognized the importance of the redistribution of electrons over the respective s and d valence atomic orbitals on the transition metal when a chemical bond is formed. It also provided the insight that electrons redistribute over the ground state and excited states of the adsorbate when a strong adsorbate bond is formed. Pettersson et.al.[11]also emphasized strong rehybridization in molecules as CO when adsorbed to the transition metal surface. The work by Triguero and Pettersson et.al.[49] demonstrated that the state of the adsorbed molecules can be different from the ground state and may even change spin multiplet state.

We will see that for atop adsorbed species there are remarkable similarities in bond energy trends of molecules and adsorbates, but that for adsorbates of high coordination significant differences arise.

In section II we will present the calculated adsorption energy trends of H, C and O adsorbed to different surface sites. They are compared with the bond energy trends of the corresponding single transition metal atom molecules.

This section will be followed by sections III and IV that analyze the electronic structure of the ad atom chemical bond and that of the transition metal molecules. The electronic structural differences are discussed to explain the different trends in bond energies of section II. Section IV also contains a

Born-Haber analysis of the adsorption energy that gives insight into which bond energy contributions dominate the differences between the transition metal atom molecules and the adsorbates.

In section V the scaling rules of adsorption energies will be compared with the bond energies of the corresponding molecules. This part contains a detailed discussion of the electronic reasons for the change in relative bond energies of the M-C bond versus that of M-CH when early and late transition metals are compared.

The paper contains a final concluding section that summarizes the results and insights obtained.

II. Trends in adsorption energies of H, C and O

The first part of this section considers the interaction energies of the H,C and O atoms adsorbed to the surface of different transition metals The second part of the section concerns the bond energies of complementary transition metal molecules. We will note analogous behavior of the energy trends for atop adsorbed ad atoms and the bond energies of the transition metal molecules. For the same transition metal the latter bond energies are stronger than the former.

The trends of the ad atom energies of H, C and O when transition metal is varied are illustrated in Figure 1. The adsorption energies on the dense (111) surface of the transition metals are studied assuming the face centered cubic structure. The adsorption energies are defined as the energies of the interacting system minus the energies of the separate systems.

The ad atoms are positioned atop in a one fold coordination site or in the threefold coordination sites. The ad atom interaction energies of 4th row and 5th row transition metals are separately considered.

Especially for H we find a very different adsorption energy trend for atop and high coordinated ad atoms. Whereas the energies of adsorption are substantially stronger, the energy trends of C adsorption have features similar to those of adsorbed H. The adsorption energies of O show a very different trend. They uniformly decrease when transition metal position moves from left to right along a row of the periodic system.

We can distinguish therefore two prototype interaction energy trends. One is representative for atop adsorbed H, the other for adsorbed O.

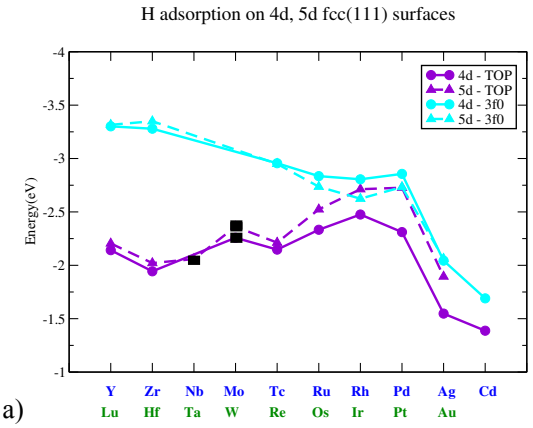

a)

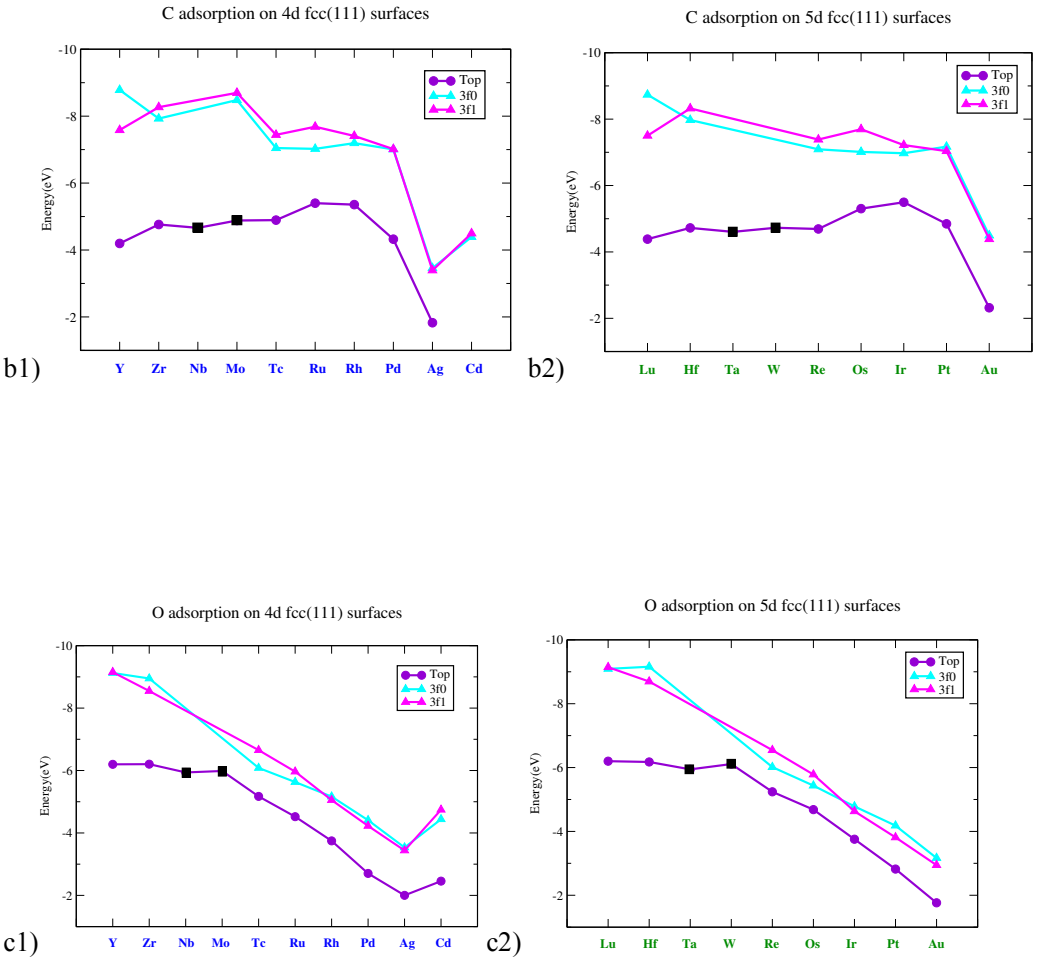

Fig.1 Trends in adsorption energies for the H, C and O ad atoms atop and threefold adsorbed on the (111) surfaces of the 4th row and 5th row transition metals. On the (111) surfaces the 3f0 fcc site has no transition metal below its center in the second row, while the 3f1 hcp site has one transition metal below its center in its second layer. All calculations have been done for the fcc crystal structures of the transition metals. Exceptions are indicated with black squares for calculations of atop adsorption on bcc (110) surfaces. a) Adsorption energies of H on the 4d and 5d transition metal surfaces; b1) Adsorption energies of C to the 4d transition metal surfaces. b2) C atom adsorption to the 5d transition metal surfaces; c1) Adsorption energies of O to the 4d transition metal surfaces; c2) Adsorption energies of O to the 5d transition metal surfaces.

We observe that atop adsorbed H (Figure 1) shows a maximum in adsorption energy for the late transition metals with nearly completely filled d-valence electron occupation. On the 4-d transition metals its energy of adsorption then approaches that of threefold adsorbed H. On the 5-d transition metals the interaction energy of atop adsorbed H can even become larger than that of threefold adsorbed H.

For the early transition metals the adsorption energies of threefold adsorbed atoms tend to increase when d-valence electron occupation decreases. This is different from expectation based on the rigid band model of the covalent adsorbate chemical bond. As we will discuss in the next section it is due

to the increasing polarity of the ad atom H bond, when attached to the low work function early transition metals.

There is an increasing energy gap on the early transition metals between the adsorption energies of more strongly adsorbed threefold coordinated H versus that of atop adsorbed H. We will see that the chemical bond of H adsorbed atop remains largely covalent and hence continues to decrease with decreasing electron population of its bonding molecular orbital partial density of states. In contrast the different bond energy trend of threefold adsorbed H is dominated by its increasing bond polarity

Very different are the trends in adsorption energy of atop and threefold adsorbed O as a function of the electron occupation of the transition metal d-valence electron band (Figures 1c). In this case the high coordination site is always preferred. Now the adsorption energies uniformly increase when transition metals valence band electron occupation decreases.

The trend in adsorption energies of C (Figure 1b) shows intermediate dependence on transition metal d-valence electron band occupation. High coordination is always favored, but the adsorption energies of atop and three fold coordinated C follow energy trends that are more similar with those of H.

Trends of the DFT calculated bond energies of the single transition metal molecules of H, C and O are shown in Figure 2.

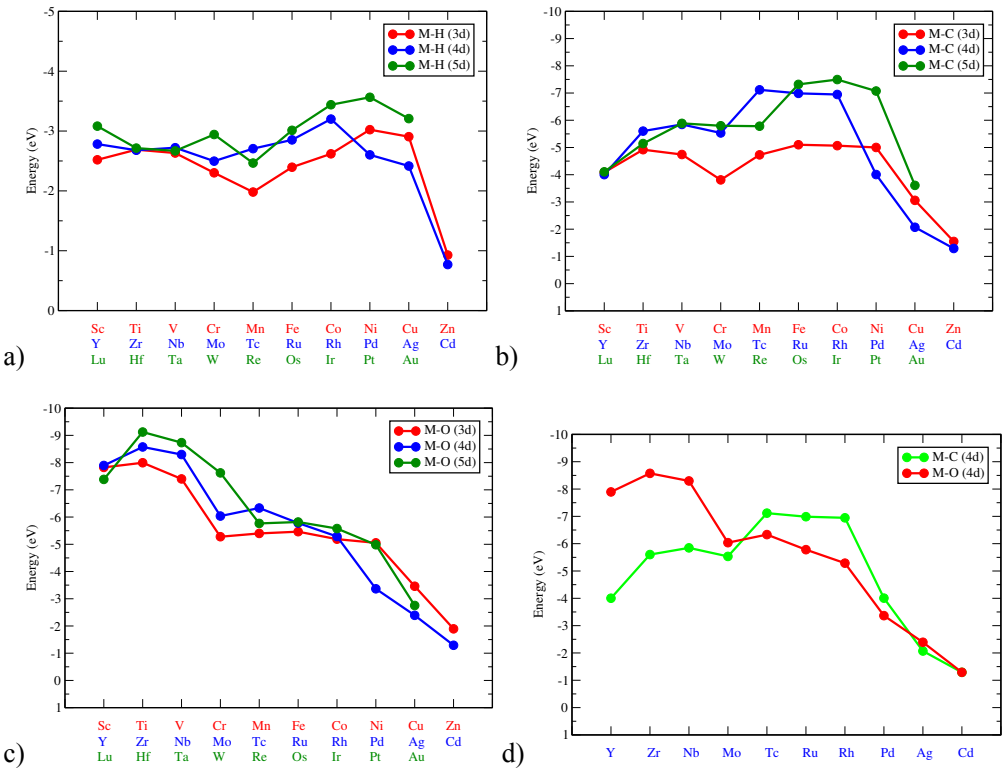

Fig.2 The molecular bond energies of the MX molecules with the transition metal atoms from the 3rd, 4th, and 5th rows of the transition metals. a) X is hydrogen; b) X is carbon; c) X is oxygen; d) Comparison of trends of C and O molecular bond energies for the 4d transition metal molecules.

The molecular bond energies are generally higher than those of the ad atoms adsorbed atop to the transition metal surfaces. The molecular MH bond energy is approximately 50 kJ/mol higher than that of the corresponding atop adsorbed H atom. For C and O the difference in energies is of the order of 100 kJ/mol. The bond energies of H are substantially lower than that of C and O. Noteworthy is the much larger variation in bond energies of the M-O bond than that of the M-C bond.

In the case of atop adsorbed C and O and for the corresponding molecules, the respective bond energies cross at a different transition metal than for the threefold adsorbed ad atoms. For the threefold adsorbed ad atoms the bond energies become equal only for an early transition metal far at the left of a row of the periodic system.

The electronic reasons for these differences are discussed in detail in section III.

The dip in the molecular bond energies for H, C and O when transition metal valence electron count is around six does not relate to the intrinsic bond strength but has to be considered an artefact. It is due to the high spin state of the reference transition metal atoms that leads to a significant exchange energy stabilization of these atoms. As a consequence the bond energies appear artificially weakened.

A similar dip in the trend of the cohesive energies of the transition metals is found when they are plotted as a function of their position along a row of the periodic system[50]. It is because the cohesive energy is calculated with the energy of reference transition metal atoms that are spin polarized. When, instead the energies of the respective transition metal atoms in their minimum spin multiplet state are considered as reference the dip in cohesive energy disappears.

Similarly for the transition metal atom molecules, when the bond energies are also calculated with respect to the reference atom in its lowest multiplet state, the dips in the bond energy plots disappear. Such corrected values for the bond energies of the transition metal molecules are given in figures 3a and 3b for the M-C and M-O bond energies of the 4th row transition metals respectively. In figure 3c the vibrational frequencies of the respective molecules are given. The vibrational frequencies are independent of reference atom. Figures 3 show that the corrected bond energies as well as vibrational frequencies show a maximum as a function of position of the transition metal along a row of the periodic system. The transition metal positions of the bond energy maxima are close to those of the respective atop adsorbed ad atoms. No dip is found anymore.

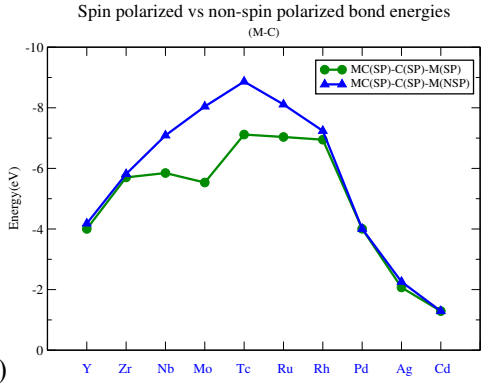

a)

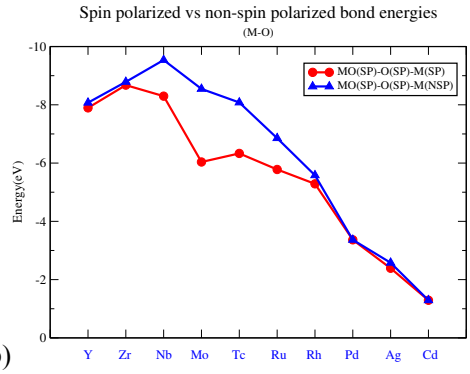

b)

c)

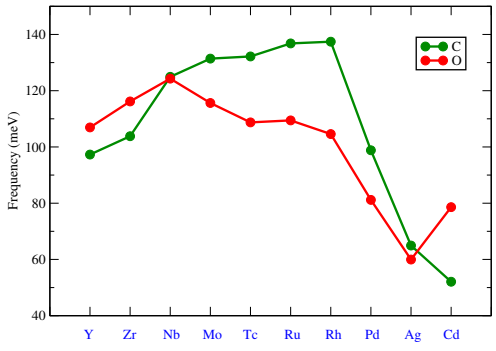

Fig.3 Comparison of reference atom spin corrected bond energies (SP) and reference atom non spin corrected bond energies (NSP) for the 4rd row transition metal molecules; a) M-C molecules; b) M-O molecules; c) Trends in calculated vibrational frequencies for the M-C and M-O transition metal molecules of the 4th row. The spin states for the spin polarized ground states of the MC molecules from YC to CdC are respectively:1,0,1,2,3,2,1,2,1,2 ;the spin polarized ground states of the MO counterparts are respectively:1,2,3,4,5,4,3,2,1,0.

In summary: Adsorption energy trends for atop and threefold adsorbed atoms are different and depend on the ad atom. For atop adsorbed species the bond energy is weaker than that of the corresponding transition metal molecules. As is illustrated in figure 4 for the interaction with N atoms there is an approximate parallel in bond energy trends between the molecular bond energies and the bond energies of atop adsorbed ad atoms.

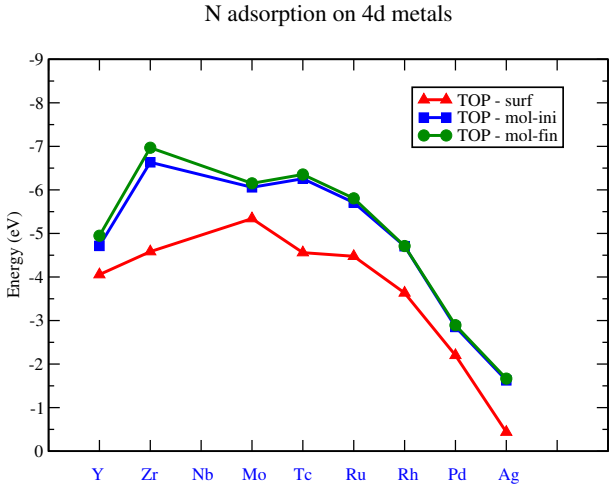

Fig.4 Comparison of interaction energies of the atop adsorbed N atom (TOP) with bond energies of the corresponding molecules. Mol-fin, indicates the energy of molecule at equilibrium distance, mol-ini indicates bond energy of molecule with MH distance similar to that of the ad atom. The molecular energies have been computed with reference to the spin polarized transition metal atoms.

III. The valence electronic structures of adsorbed H, C and O

In this section the electronic features of atop and threefold coordinated ad atoms to the (111) surfaces of transition metals of fcc structure are compared. We have seen in the previous section that adsorption energy trends may not only be different when adsorbate is varied, but for the same

adsorbate may vary for different adsorption sites. The analysis of this section focusses on the electronic cause of these differences.

We will calculate the respective partial densities of states (PDOS) that give the electron distribution over the respective atomic orbitals and will base our analysis also on computed crystal orbital Hamiltonian overlap population densities (COHP) that provide information on the electron energy distribution over bonding and antibonding molecular orbital electron densities. The PDOS and COHP are defined is section VII. We will also discuss the consequence of varying balance of covalent and ionic contributions to the bond energy due to variation in chemical bond polarity

An adsorbate on a different site interacts with different combinations of surface transition metal atomic orbitals. For instance, because of symmetry, the s- atomic orbitals of the threefold adsorbed atom will only interact with a symmetric combination of the s-atomic orbitals located on the three surface transition metal atoms. This linear combination of surface atomic orbitals is called a surface group orbital[51–53].

The adsorbate atomic orbitals project on different group orbitals of the atomic orbitals of the surface metal atoms that interact with the adsorbate. This is the origin of the difference in ad atom bond energies on different adsorption sites.

In figures 5, 7 and 8 we compare the calculated electronic structures of the chemical bonds of H, C and O adsorbed to the Rh(111) surface. In figure 7 a comparison of C adsorbed to Rh(111) with C adsorbed to Tc(111) is included.

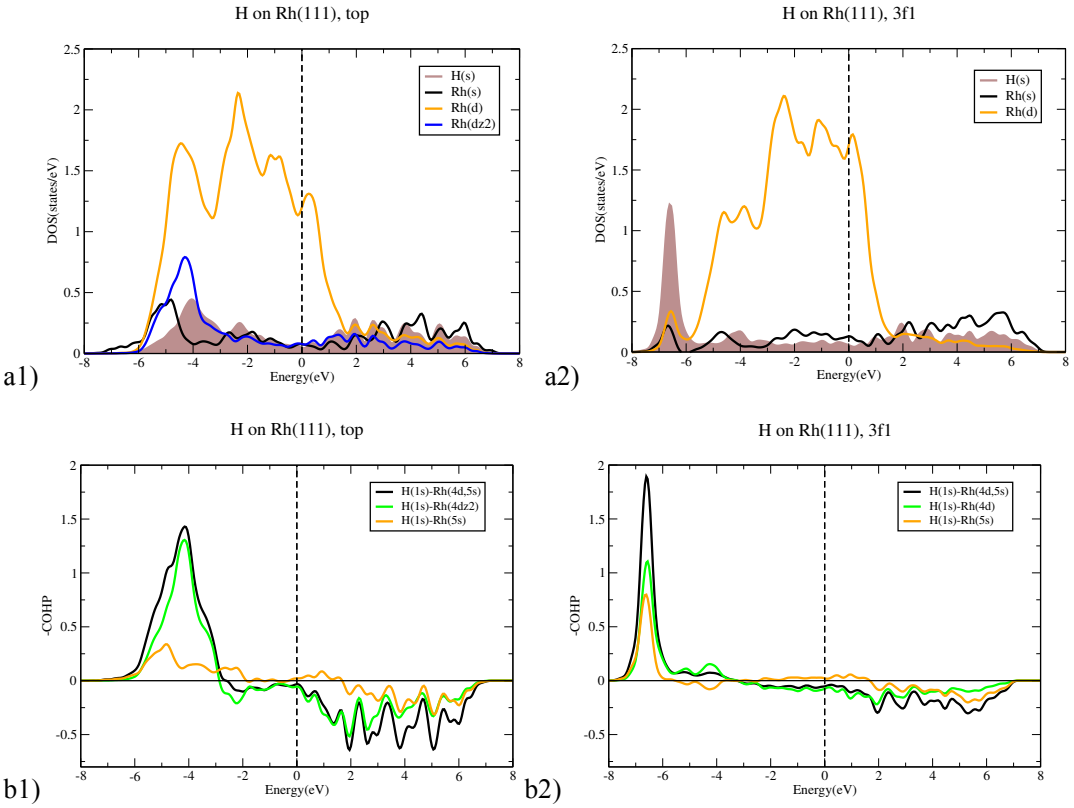

Fig.5 The valence electronic structures of the H ad atom adsorbed to the Rh (111) surface. a1) PDOS of atop; a2) and threefold adsorbed H; b1) -COHP of H atom adsorbed atop; b2) adsorbed threefold;

In figures 5a, 7a and 8a the respective PDOS of the atomic orbitals on the adsorbate and of the transition metal valence electron atomic orbitals are shown. One clearly distinguishes the broad and large intensity of the transition metal d-valence electron band that is nearly completely electron occupied. The PDOS intensity of the transition metal s-valence electron band is much smaller. In the transition metals the electron occupation of the transition metal s-valence electron band is approximately constant. It varies around one electron per transition metal atom.

Near the bottom of the d-valence atomic orbital electron band in figure 5a1 one notes the presence of the PDOS for the H 1 s atomic orbital. For three fold adsorbed H the interaction with the surface is stronger, and in figure 5a2 the peak belonging to the H 1s atomic orbital PDOS appears below the d-valence electron band.

The PDOS of the ad atom chemical bond consists of electron energy density distributions with a large energy separation Δ between the average bonding and antibonding molecular orbital partial densities of states. The bonding or antibonding nature of the molecular orbital partial density of states is deduced from the COHP plots shown in figures 5b, 7b, 7c and 8b respectively. When –COHP is positive the molecular orbital partial density of states of the chemical bond is bonding, when –COHP is negative it is antibonding. In between, zero values of –COHP indicate a nonbonding electron density region

With the help of COHP's the respective bonding and antibonding molecular orbital partial density of states of the ad atom surface chemical bond can also be identified in the PDOS for C and O. They appear as peaks near the bottom edge and the top edge of the d-valence electron bands respectively.

In between the bonding and antibonding molecular orbital partial density of states there is sometimes a rather flat nonbonding density of states region. When the Fermi level is located in this partial density of states region variation of d-valence electron occupation will alter the adsorption energy little.

The rigid band model can be used to extrapolate from the known electronic distribution of the chemisorptive bond on one transition metal surface to that of another metal[1]. It assumes that the transition metal density of states distribution does not differ and that the interaction with the metals s-valence electrons does not change.

Then trends in adsorption energy only vary by a change in transition metal valence electron occupation that as we explained in the introduction relates to the average position of the d-valence electron band energy ξ_d with respect to the Fermi level. For this reason the rigid band model is also called the d-band shift model [21].

As can be observed from a comparison of figures 7b and 7c, notwithstanding some small differences of their respective PDOS's and the shift in Fermi level because of the altered electron occupation, the electronic structures of the chemical bonds of C adsorbed to Rh and Tc appear to apply reasonably well to the rigid band model.

A maximum in bond energy is predicted when the Fermi level is located in the nonbonding molecular orbital partial density of states of the chemical bond. At low valence electron occupation only bonding molecular orbitals are occupied. When electron occupation increases (or Fermi level moves to higher electron energies) the bond strength will increase until the nonbonding molecular orbital partial density of states is reached. The bond strength will decrease when antibonding molecular orbitals levels become occupied.

The different dependence of the adsorption energies of atop and threefold adsorbed ad atoms on valence electron occupation can be explained using the schematic PDOS and COHP plots of figure 6.

At low d-valence electron occupation only the bonding molecular orbital partial density of states is electron occupied. Because of its lower electron energy the fraction of electron occupied bonding molecular orbital partial density of states is higher for threefold adsorbed H than for atop adsorbed H. Therefore three fold adsorbed H will have a stronger bond energy with the surface.

When electron occupation increases the change of Fermi level energy position from bonding to antibonding molecular orbital partial density of states depends on adsorption site. It shows the average lower energies of the PDOS of the atomic orbitals of threefold adsorbed ad atom compared to atop. For atop adsorbed H the molecular orbital partial density of states will remain bonding at a higher electron energy than at threefold position.

This can be also seen from the calculated results in figure 5. For H three fold adsorbed on the Rh(111) surface the Fermi level is located in the antibonding molecular orbital partial density of states whereas for atop adsorbed H the Fermi level is located close to the non- bonding molecular orbital partial density of states.

When with a change in transition metal valence electron band occupation the Fermi level changes position from the bonding to antibonding molecular orbital partial density of states the bond energy will decrease. It causes a decrease in the relative interaction energy of threefold compared to that of atop adsorbed H.

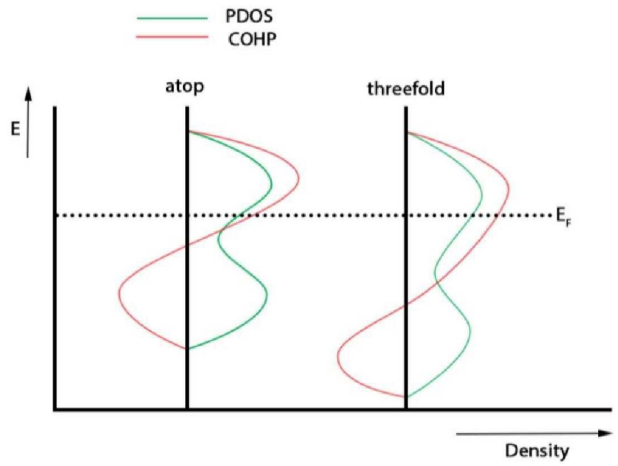

Fig.6 Schematic PDOS plots (blue) and -COHP plots (red) of the electronic structure of the chemical bond formed by σ symmetric molecular orbitals between adsorbate atomic orbital and transition metal atomic orbital as a function of electron energy. a) atop adsorption; b) adsorption in high coordination site. Note that for clarity in this figure we have plotted +COHP instead of –COHP, in this figure only.

The energy trends of the bond energies of atop and threefold adsorbed H ad atoms to the late transition metals are explained well by the rigid band model of the electronic structure of their chemical bonds.

However the bond energy increase for threefold adsorbed H when position of the early transition metals moves to the left along a row of the periodic system cannot be explained within the covalent rigid band model, but as we will discuss below is due to the increasing polarity of the M-H bond.

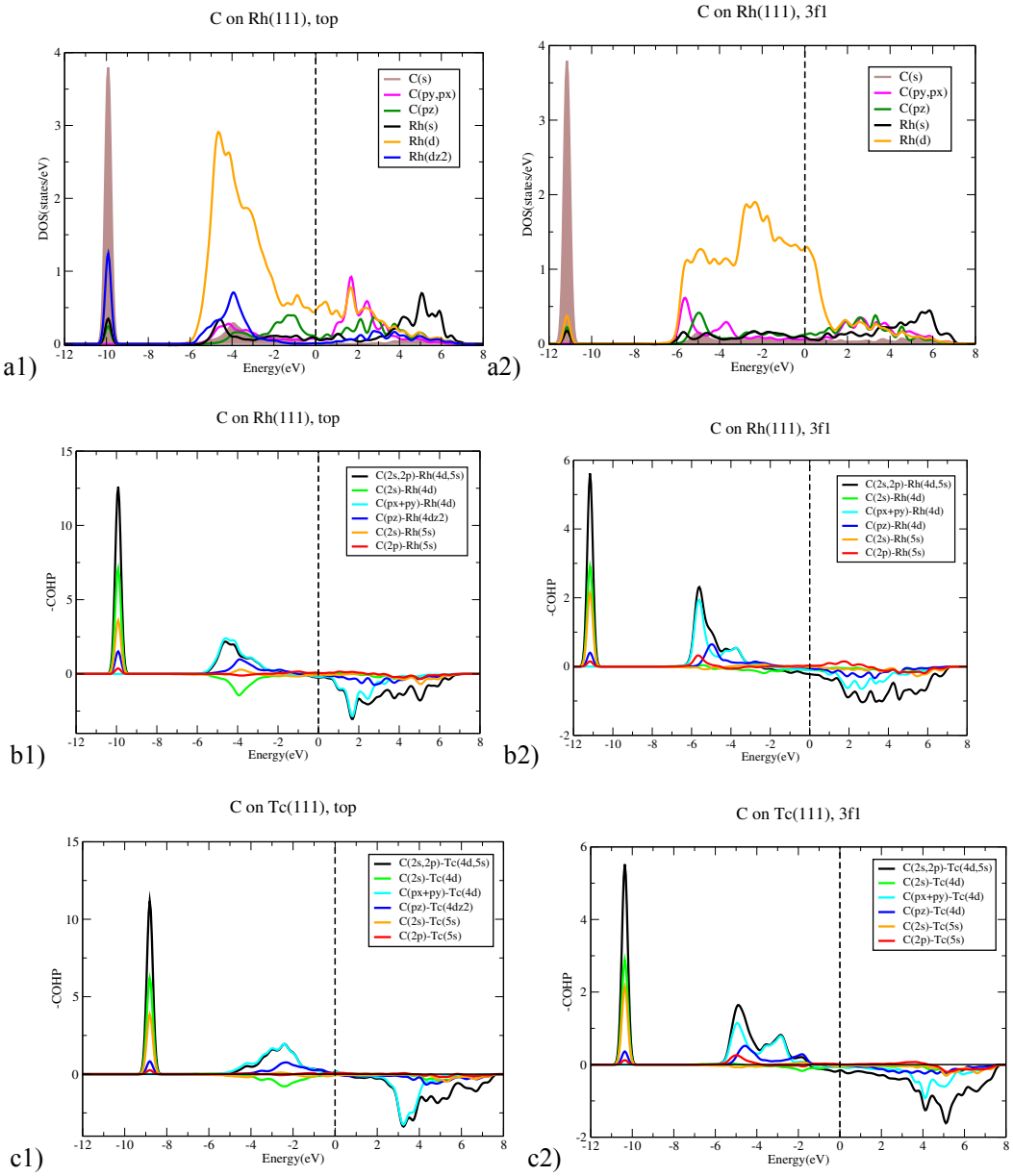

Fig.7 The electronic structures of C adsorbed to the Rh and Tc (111) surfaces; a1) PDOS of C atom atop adsorbed to the Rh surface; a2) PDOS of C threefold adsorbed to Rh surface; b) -COHP of C atom adsorbed to the Rh surface; b1) atop; b2) threefold; c) -COHP of C atom adsorbed on the Tc surface; c1) atop; c2) threefold.

An important difference between C, O and H is the presence of more valence atomic orbitals on the former two atoms. The C and O atom contribute one 2s and three 2p atomic orbitals, compared to the 1s atomic orbital of the H atom. The 2s and $2p_z$ atomic orbitals are σ symmetric with respect to the surface normal. Two of the 2p atomic orbitals are π symmetric with respect to the surface normal, so that different orbital symmetry interactions become possible compared to H adsorption. This causes the strength of the chemisorption bonds to be substantially stronger for C and O than for H.

In figures 7 and 8, below the d-valence electron band a sharp feature in the PDOS appears that is due to the interaction with the C 2s atomic orbitals. The small contribution of the transition metal atomic

orbitals to this peak implies that they interact only weakly. The main contribution to the chemical bond is due to the interaction with the ad atom 2p atomic orbitals. The PDOS of the ad atom 2p atomic orbitals are located at higher energies and overlap partially with the d-valence electron energy density. The corresponding COHP curves show two major peaks that can be interpreted as the respective bonding and antibonding molecular orbital partial density of states of the respective chemical bonds.

The maximum of the bonding molecular orbital density of states is close to the bottom of the d-valence electron band, the maximum of the antibonding molecular orbital density of states appears near or above the upper transition metal d-valence electron band edge.

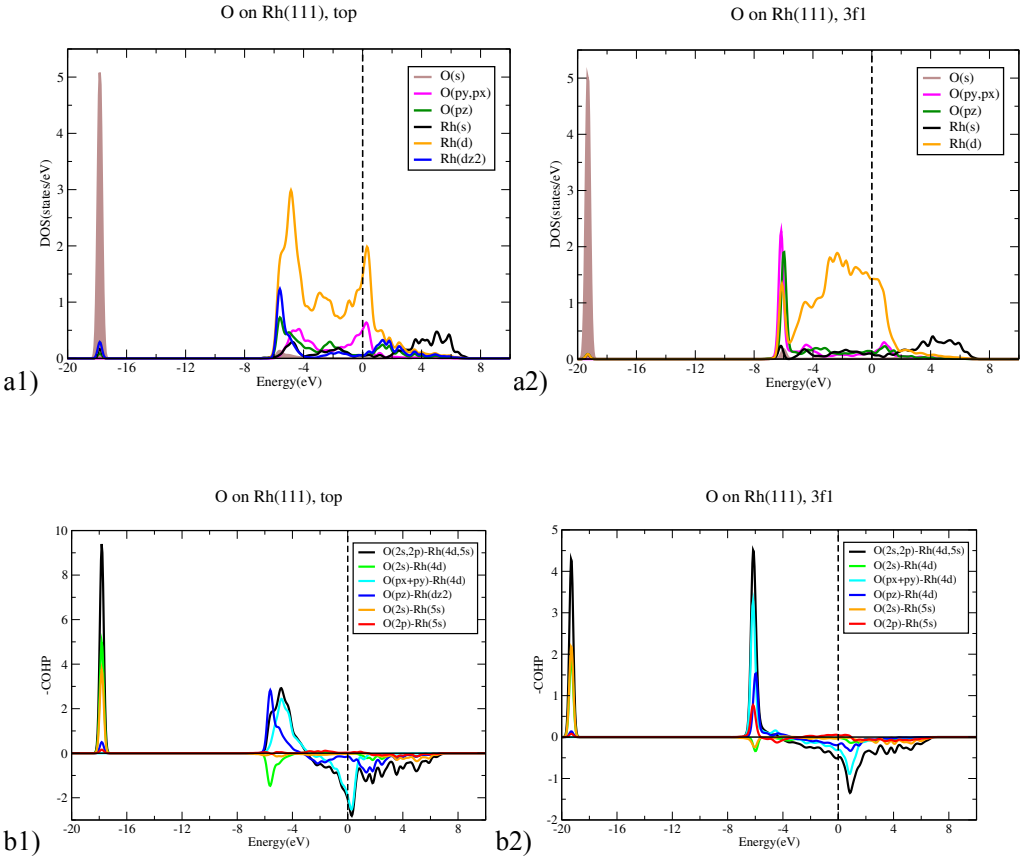

Fig.8 The electronic structures of O adsorbed to the Rh(111) surface: PDOS of O ad atom adsorbed a1) atop and a2) threefold; -COHP of O atom adsorbed b1) atop b2) threefold

The π symmetric molecular orbital interaction is stronger than the σ symmetric molecular orbital interaction. As can be observed from the respective PDOS's and COHP's it is shifted more downwards in energy. For the threefold adsorbed ad atoms the π as well as σ symmetric molecular orbital densities shift downwards in energy. Compared to the chemical bond of the atop adsorbed ad atoms the chemical bond of threefold adsorbed atoms shows a substantial increase in polarity. This polarity of the chemical bond is larger for O than for C and can be deduced from the large increase of the 2p atomic PDOS's in the respective bonding molecular orbital density of states. It is due to increased back donation from the transition metal surface into the ad atom 2p atomic orbitals. The corresponding charge increases on the ad atoms are given in table 1. The higher polarity of the threefold adsorbed ad atoms compared to that of the atop adsorbates implies a substantially larger

ionic contribution to the chemical bond. This gives an extra stabilization of the bond energy of the threefold adsorbed species.

The larger effective nuclear charge of O compared to that of C, causes the O atomic orbitals to be located deeper in energy with respect to the Fermi level and hence the antibonding molecular orbital density of states of the M-O chemical bond is more occupied. When adsorbed to the late transition metals, notwithstanding its higher charge, the bond energy of O is weaker than that of C (see fig 1b and c) because of the larger Pauli repulsion experienced by the former. The steeper increase of the M-O bond energy than that of C when transition metal d-valence electron occupation decreases is due to the depopulation of antibonding electron energy density in the M-O chemical bond. For the early transition metals the increasing polarity of the M-O bond leads to an additional increase of the ionic energy contribution to the chemical bond energy

For three fold coordinated H, C and O the increase in bond energy when attached to the early transition metals is due to the dominance of the ionic contribution to the bond energy

Quantitative information on the polarity of a chemical bond is deduced from Bader charges [54] and from topological electron density properties such as the Laplacian and electron density at bond critical point [55] collected in Table 1. The Bader charges are a measure of the electron occupation of an atom. When the Laplacian value at bond critical point is negative the bond can be considered covalent, when it is positive it is to be considered ionic. The electron density values at bond critical point are a measure of the bond order of the chemical bond. It probes the covalent energy contribution to the chemical bond.

The table illustrates the differences in electron transfer between atop and threefold adsorbed C, O and H adsorbed to the Rh(111), Tc(111) and Zr(111) surfaces.

	H			**C**			**O**		
	Chg	Lpl	Eld	Chg	Lpl	Eld	Chg	Lpl	Eld
Zr top	-0.533	1.214	0.521	-1.096	8.948	1.073	-1.039	14.054	1.399
Zr 3f1*	-0.697	2.348	0.332	-1.796	3.493	0.774	-1.323	7.483	0.677
Tc top	-0.250	-0.624	0.809	-0.432	-2.586	1.690	-0.705	17.371	1.934
Tc 3f1	-0.338	3.103	0.477	-0.821	8.825	1.038	-0.944	10.876	0.838
Rh top	-0.070	-2.631	1.033	-0.088	-3.945	1.874	-0.596	17.432	1.517
Rh 3f1	-0.143	2.906	0.550	-0.394	2.768	1.141	-0.729	10.291	0.837

Table 1 The Bader charges (e.u.), the Laplacian values and electron density values at bond critical points for C, O and H adsorbed atop and threefold to the Rh(111), Tc(111) and Zr(111) surfaces. Chg is Bader charge, Lpl is laplacian value at bond critical point and Eld is electron density value at bond critical point. Note that the Laplacian and electron density for threefold sites have been calculated between ad atom and a single surface metal atom and cannot directly be compared with the values of atop adsorption. The Laplacian is the sum of the three eigenvalues of its Hessian matrix. * The three fold adsorbed C atom is located interstitially.

The bond orders (Eld) of H and C uniformly decrease when transition metal valence electron count decreases, but that of O has a maximum. This is for H and C due to reduction of electron occupation in the bonding molecular orbital density of states. When O is attached to Rh the Fermi level is located in the antibonding molecular orbital density of states. Therefore with a decrease of electron occupation the bond order will initially increase. The bond order will decrease only once electron occupation of bonding electron energy density decreases.

The topological electron density data in Table1 of H and C adsorbed atop to Rh and Tc surfaces show that the laplacian is negative. This indicates that the respective chemical bonds are covalent. In this case the electron density differences (Eld) give the proper ranking of bond energies. Atop adsorbed H and C bind stronger to the Rh surface than to Tc surface.

However for three fold adsorbed H, C and O the sign of the Laplacian indicates a polar bond. Therefore the bond order estimates based on the electron densities of Table 1 that relate to the covalency of the chemical bond cannot be used to predict the adsorption energy trends of Tc or Zr. The respective bond energies increase and their trend relates to the increasing charge on the ad atoms.

In summary: Bond energy trends relate to the position of the Fermi level in the molecular orbital density of states of the chemical bond as long as the polarity of the chemical bond is not too large. Beyond a particular bond polarity the adsorption energy will increase with increasing electron transfer to the adsorbate. This can counteract bond energy trend predictions based on the rigid band model.

For H and C the different bond energy trends of atop and threefold adsorbed ad atoms on the early and late transition metals are due to the differences in the polarity of the respective chemical bonds. When atop adsorbed the covalent interaction tends to dominate, whereas when threefold adsorbed the ionic interaction becomes dominating.

IV Comparison of bonding in single transition metal atom molecules and that of the chemisorptive surface bond; the Born-Haber cycle of adsorption.

The essential difference between the electron distribution in molecules and of the ad atom adsorbed to a metal surface is that the valence electron distribution at the transition metal surface is continuous, whereas in the molecule the electron density distribution is discrete. The degree of broadening of the molecular orbital partial density of states in the solid is a measure of the degree of electron delocalization with the surrounding transition metal atoms. This is the electronic cause of the weaker bond energy of the ad atom compared to that of the molecule.

The other effect of the broadened partial density of states is a spreading of the bonding and antibonding molecular orbital partial density of states over a larger energy density region. It may lead to overlap of the molecular orbital partial density of states that is mapped on the molecular orbitals of the non-interacting molecule. The latter affects hybridization largely. It is one of the reasons that

details in trends of bond strength as a function of transition metal valence electron band occupation may differ for ad atoms compared to that of the transition metal molecules.

An elementary view of the energy cost of electron delocalization is competition of surface atom electrons for binding to the ad atom or with neighbor transition metal atoms. This we will illustrate by a Born –Haber analysis of adsorbate formation in section IVB. Before this, in section IVA we will discuss the electronic structure of the chemical bond of the single transition metal atom molecule.

In the next section IVA we will discuss the electronic structure of the transition metal molecules. This is a topic that has been extensively investigated with many different computational techniques since many years. Early papers are the Bauschlicher et.al. and Bagus et.al. ab initio calculations on a variety of first row transition metal hydrides[56, 57]. More recent computational and experimental papers can be found in[46, 47, 58, 59]. An early reference to calculations on TiO and FeO is [60].
We extend these studies here by an analysis of the bond order overlap densities based on calculation of the COHP's of the transition metal molecules. These will be compared with the electronic structure of the corresponding ad atoms.

IVA The electronic structure of the single transition metal atom molecule.

The electronic structure of the transition metal molecules we will introduce using the TcC molecule as an example.

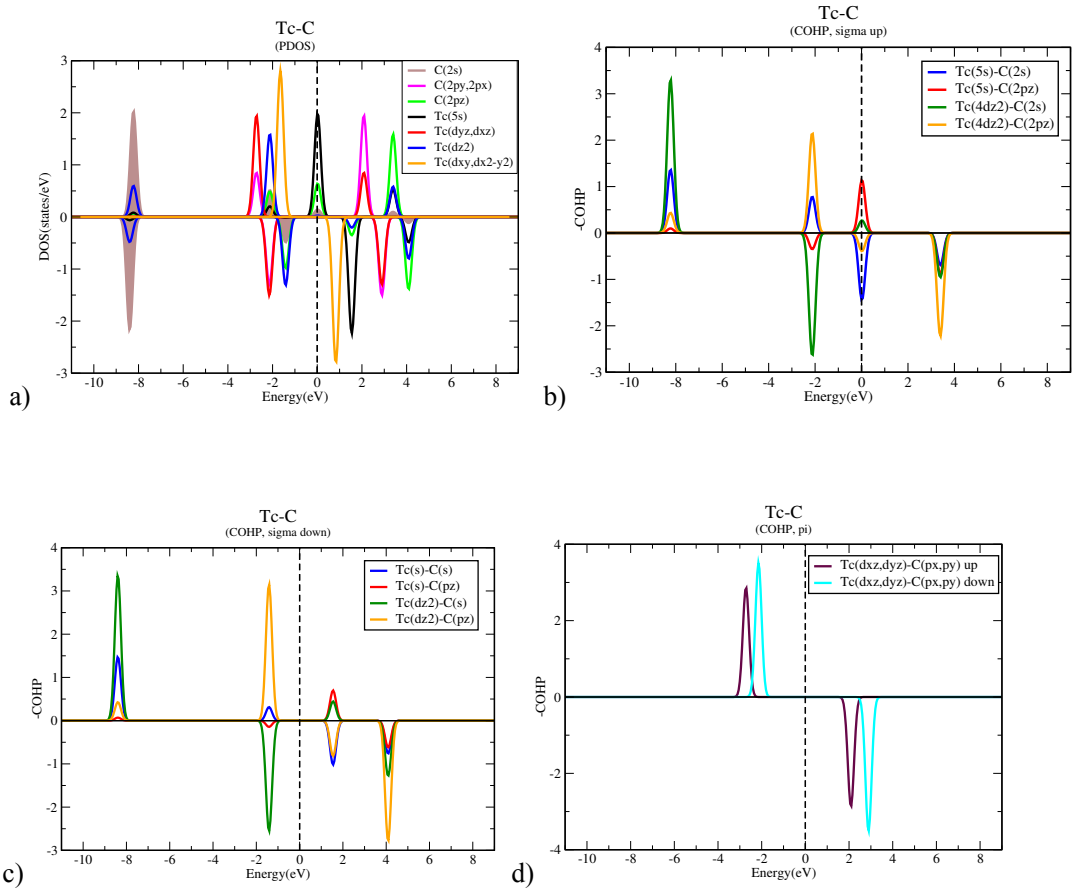

Fig.9 The electronic structure of the TcC molecule; a) PDOS, spin up with positive sign, spin down with negative sign; b) -COHP for σ symmetric molecular orbitals with spin up; c) -COHP for σ symmetric orbitals of spin down; d) -COHP for π symmetric orbitals, spin up and spin down.

Figures 9 illustrate that the valence electron structure of the molecule is composed of 4σ and 4π symmetric molecular orbitals and two non-bonding metal d-atomic orbitals of δ symmetry. Often the molecules have high spin so that the orbital energies depend on electron spin, the molecular orbital number doubles and each molecular orbital then contains one electron. The respective spin states of the ground state of the carbide and oxide molecules are mentioned in the legend of figure 3. It is maximum when the nonbonding δ symmetric orbitals are partially occupied.

In the case of the TcC molecule, five of the total number of 11 electrons are distributed over three σ symmetric spin up and two σ symmetric spin down orbitals, four electrons occupy bonding π orbitals and two electrons are contained in degenerate d_{xy} and $d_{x^2-y^2}$ orbitals. The spin state of the TcC molecule is a quartet. The HOMO is σ symmetric and contains one electron. It is slightly antibonding.

Of the four σ symmetric molecular orbitals(fig 9b;fig 9c) one is a bonding orbital of low energy, and at increasing energy there are two orbitals, that show weakly bonding or antibonding features, and a fourth antibonding molecular orbital. For the transition metal molecules the actual nature of the two intermediate orbitals depends strongly on the hybridization of transition metal atom (n+1)s and (n) d atomic orbitals.

Similarly as for the adsorbed state, the strong bond in the M-C molecule is due to the occupation of the bonding π symmetric molecular orbitals that remains largely unchanged when the transition metal is changed, except when the transition metal atom gets high d-valence electron occupation. Changes in bond energy for molecules with a different transition metal atom are mainly due to variation in the occupation of molecular σ symmetric orbitals or due to variation of exchange energy stabilization when electron occupation of the nonbonding orbitals varies.

When electron number of the MC molecule varies, the bond strength and changes in electron occupation only occur in the non-bonding δ symmetric orbitals. Therefore the bond energy will mainly change due to altered spin exchange energy stabilization. This is observed in figure 3a where the TcC bond energy becomes larger than that of the RuC bond due to this exchange energy stabilization.

The electronic structures of TcC, RuC and RhC are compared in figures 10. In these molecules there is only a change in the electron occupation of the nonbonding δ symmetric atomic orbitals. Similarly, for C adsorbed to Tc, Ru or Rh surfaces the Fermi level is located in the nonbonding electron energy density region of the ad atom-surface chemical bond.

The HOMO of these transition metal molecules is a single electron occupied σ orbital. The relative energies of δ and σ orbitals however changed in RhC, because the higher nuclear charge on Rh lowers the relative energies of the d-atomic orbitals. The middle σ orbital becomes antibonding because of this change in hybridization. This causes the bond energy of RhC to decrease. The increase in bond energy from MoC to TcC is due to the additional population in TcC of a slightly bonding middle σ symmetric molecular orbital.

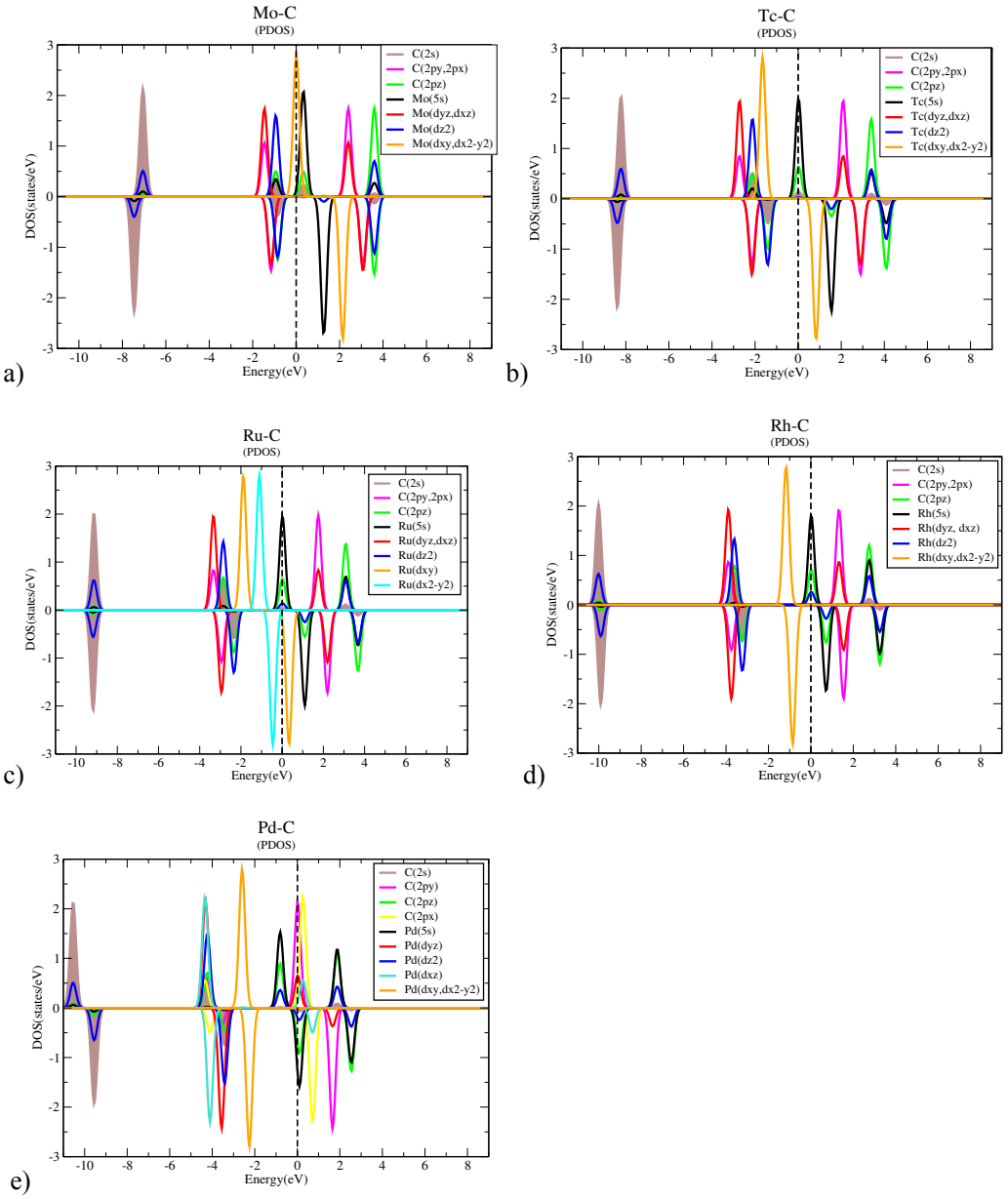

Fig.10 The PDOS, spin up with positive sign and spin down with negative sign, of the a) MoC; b) TcC; c) RuC; d) RhC; and e) PdC molecules.

The reason for the steep decrease in bond energy of the PdC bond compared to that of RhC is because an additional electron occupies the antibonding π orbital.

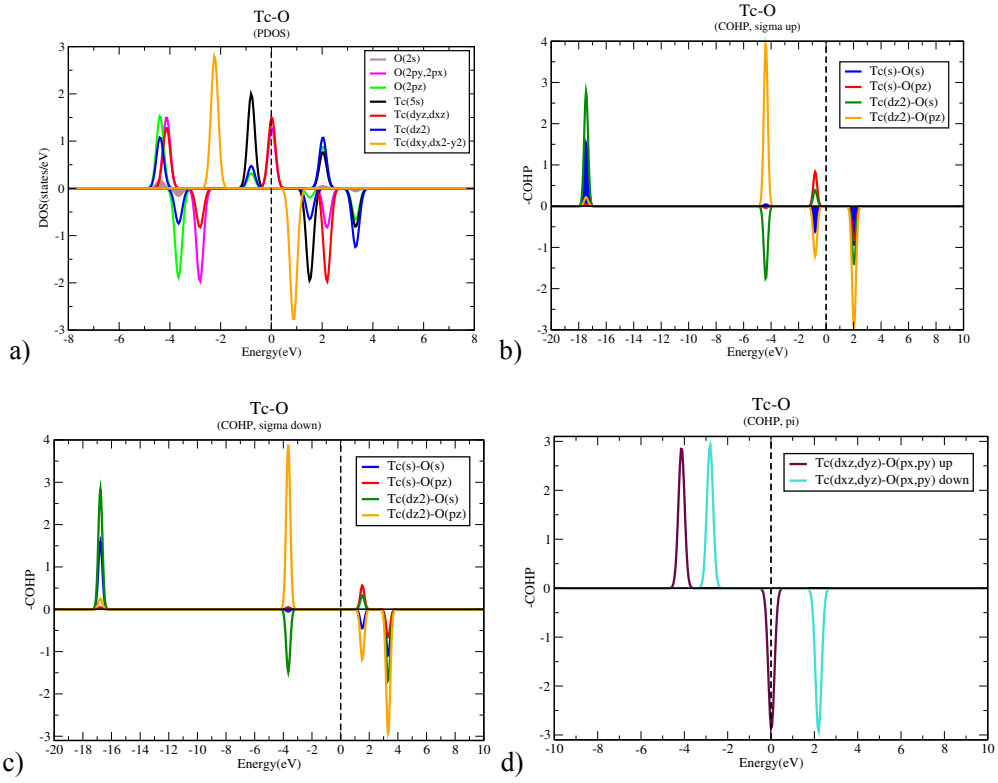

Fig.11 The electronic structure of TcO. a) PDOS, spin up with positive sign, spin down with negative sign ; b) -COHP of σ symmetric orbitals (spin up); c) -COHP σ symmetric orbitals (spin down); d) -COHP π symmetric orbitals, spin up and spin down.

In figures 11 the electronic structure of the TcO molecule is shown. As expected the orbital structure is similar to that of the TcC molecule, but distribution of electrons is different. Because of the lower energies of the O atomic orbitals and the additional two electrons in TcO compared of the TcC molecule the HOMO is now one of the antibonding π orbitals.

Instead of the discrete energies in the molecule, on the surface the PDOS have a broad and continuous energy distribution. Figure 12 illustrates this. It also shows the close similarity between bonding in the transition metal molecule and that of the atop adsorbed ad atom. For the RhC molecule and C adsorbed atop to the Rh surface the respective the bonding and antibonding molecular orbital partial density of states are compared. The valence electron energies are in comparable electron energy intervals. The distribution of electron density over bonding and antibonding orbital density of states is also closely related. In both cases one notes the larger intensity of the π symmetric interactions compared to the σ symmetric interactions that indicates the dominant contribution of the π symmetric orbital interactions to the bond energy.

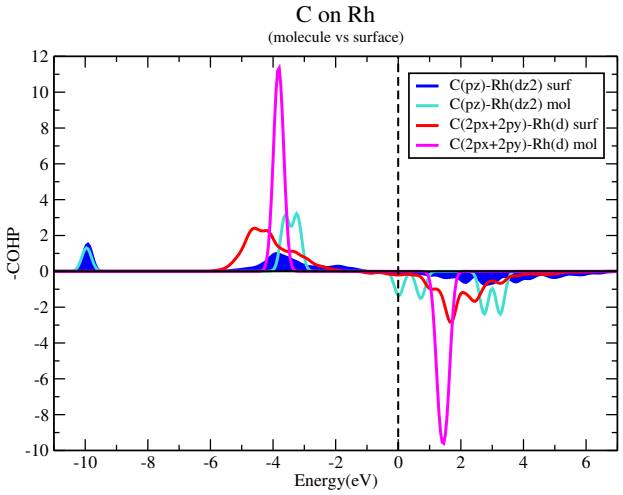

Fig, 12 Comparison of the COHP's of the RhC molecule and C ad atom adsorbed atop of the Rh(111) surface.

IV B Born Haber analysis

Using a Born-Haber analysis the relative energy contributions of the metal surface –adsorbate interaction and embedding energy cost to the chemisorptive bond energy can be estimated. We will see that the difference between the bond energies of adsorbate and that of the transition metal molecule correlates with the strength of the transition metal-atom bonds.

We will compare in detail the bond energies of the C ad atoms on the Tc and Rh (111) surfaces. This comparison is of particular interest because the bond energy of the TcC molecule is stronger than that of the RhC molecule, but the C ad atom binds stronger atop to the Rh surface.

The Born-Haber cycle analysis has been originally used to calculate from the lattice energy of ionic compounds atomistic and molecular properties as the electron affinity of their components or to make estimates of the lattice energy[61].

To calculate the heat of formation one designs a reaction cycle in which some of reaction energies are known from independent thermodynamic data. Then the value of an unknown reaction step in a proposed scheme can be estimated.

We will apply such a scheme to the adsorption process to deduce energy values for the insertion energy of a transition metal molecule into a vacant surface, that will give use the embedding energy.

The Born-Haber cycle is not unique. It can be used in different ways that depend on the reaction cycle that is proposed. For instance the Born-Haber cycle scheme has also been applied to estimate reaction energies of adsorbed species from combination of thermodynamic gas phase and adsorption data[62].

Here we apply the decomposition scheme that is schematically shown in fig. 12, to determine the embedding energy from calculated values of the molecular bond energy, adsorption energy and surface vacancy formation energies.

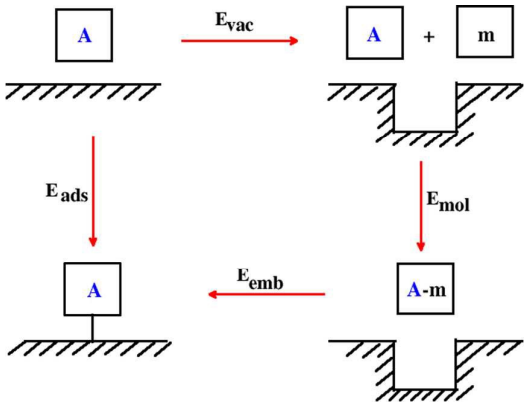

Figure 13. Schematic Illustration of the Born-Haber cycle to disentangle the energy contribution of molecular bond formation from that of its embedding energy.

To construct the adsorbed state in a first step a vacancy is created in the surface. One atom is removed when atop adsorption is studied and a three atom cluster is to be removed for adsorption in threefold coordination. The geometries remain fixed as computed for the adsorbed state. In a second step the surface complex molecule is formed. Reinsertion of the surface complex molecule into the vacant site of the surface gives the embedding energy contribution. This energy is corrected for the difference in energy of the free surface and the surface with coordinates frozen into the position of the adsorbed state. The main role of the surface is to constrain the molecular complex to the surface geometry of the embedded complex.

Atop on C	E_{ads}	E_{mol}	E_{vac}	E_{reins}	E^{s}_{rel}	E_{emb}	*Spin state*
Rh	*-5.35*	*-6.86**	*6.73*	*-5.64*	*0.42*	*1.51*	*Doublet*
			7.02	*-5.64*		*1.80*	*Doublet*
		-7.15					
Tc	*-4.89*	*-6.94**	*8.86*	*-7.19*	*0. 37*	*2.04*	*Quartet*
			10.61	*-7.19*		*3.79*	*Quartet*
		-8.68	*10.61*	*-7.61*		*3.37*	*Doublet*
		-8.26					
Threefold							
Rh_3C	*-7.40*	*-9.25**	*14.74*	*-13.07*	*0.18*	*1.85*	*Doublet***
			15.44	*13.07*		*2.55*	*Doublet*
		-9.95					
Tc_3C	*-7.44*	*-8.44**	*20.13*	*-19.36*	*0.23*	*1.00*	*Dectet****
			22.42	*-19.36*		*3.29*	*Dectet*
		-10.73	*22.42*	*-20.75*		*1.89*	*Doublet*
		-9.33					

Table 2. The Born Haber analysis of C adsorbed to the (111) surfaces of Tc and Rh. Atop and threefold adsorbed C are compared. High spin state and low state molecular energies are calculated with reference to the high spin state as well as low spin state transition metal atoms. Molecular spin states are indicated in the right column. Energies are in eV. *) Non-spin corrected reference transition metal atom. **) Spin state Rh_3 sextet. ***) Spin state Tc_3 dodecet.

Table 2 gives the different energy contributions of the Born-Haber cycle analysis for C adsorbed atop and threefold to the (111) surfaces of Tc and Rh respectively. The energy of adsorption of the C atom is equal to the energy of formation of the surface molecular chemical bond minus the embedding energy. This is the energy cost of localization of valence electrons on the surface transition metal atom that binds to the adsorbate, due to its additional binding to neighboring surface metal atoms. Since magnetic stabilization of reference transition metal atoms can be significant and adsorption energies have as reference the non-magnetic surface, comparison is made between molecular energies calculated using high spin state transition metal atoms as well as low spin state transition metal atoms as reference. When relevant also comparison is made with the molecular energy of a low spin state molecule. The latter is of interest because it enables to make an estimate of the contribution of magnetic moment quenching to the adsorption energy.

We will first compare the adsorption energies of C adsorbed atop to the (111) surface of Rh and Tc respectively. Whereas the molecular energy of TcC is larger than that of the RhC molecule, the reverse is the case for the bond energy of the adsorbed C atoms. The most important contribution to this decrease in relative energy is the increased cost of electron localization on the Tc atoms. This is larger for Tc than for Rh. The lower d- valence electron occupation of Tc reduces the electron occupation of the antibonding valence electrons in the former, that increases localization energy cost in parallel with the metal atom –metal atom interaction energies. The localization energy will weaken the M-A interaction strength of the adsorbed state with respect to the molecular bond strength and it will weaken the surface metal-metal atom interaction energies compared to those when the surface is free of adsorbate, it decreases the adsorption energy by 20% compared to the bond energy of the corresponding transition metal molecule.

Comparison of the embedding energies for the high spin state TcC molecule and low spin state TcC molecule shows that the contribution of spin quenching is only 10% of the total embedding energy.

From the data in Table 1 one observes a larger bond order for atop adsorbed C on Rh (Eld=1.894) compared to that of Tc (Eld=1.690).In agreement with the data of table 2 this indicates that the Tc-C interaction energy on the surface is the weaker. The calculated bond orders of the RhC molecule (Eld= 2.063) and TcC molecule (Eld=2.031) respectively are close in value and larger than those of the corresponding atop adsorbed atoms. This shows that when attached to the surface the bond energy of the Tc-C chemical bond has become more weakened than that of the RhC chemical bond. We have seen in table 2 that the embedding energy cost on Tc is also the larger.

When one compares molecular energies of threefold adsorbed C with the respective adsorption energies, one sees that a large part of the increase in adsorption energies is already accounted for by the increased molecular energies of the three coordinated C transition metal molecule that now contains three transition metal atoms. For the magnetic Tc_3C molecule the spin quenching contribution to the decrease in adsorption energy is now 30 % of the embedding energy.

When the embedding energy is corrected for quenching of the magnetic moments the relative contribution of the localization energy to the adsorption energy of threefold adsorbed C atom is found to be less than that for the atop adsorbed C atom. The overall result is that the adsorption energies of C in three fold coordination to Rh and Tc are comparable, but when adsorbed atop the adsorption energy of C is least on Tc.

The Born-Haber analysis of this section justifies the electronic analysis approach of section II. In this section changes in adsorbate bond energies are related only to differences in the electronic structures and electron occupation of the transition metal atom –adsorbate partial density of states. The altered electronic structure of the transition metal atom bond near the adsorption site is not explicitly considered. As we have seen in section IV A embedding of the transition metal molecule in the surface changes the PDOS's and COHP's of the metal atom-adsorbate chemical bond, that hence incorporate the effects on electronic structure due to electron delocalization of the surface valence electrons.

V. Scaling rules

Herein we will elaborate on the differences in adsorption energy trends between adsorption atop and a high coordination site. This appears also to affect the adsorption energy scaling rule. The scaling rule has been proposed by Nørskov et.al.[1, 16] and developed further by Sautet, Rossmeisl and Koper et.al.[4, 50]. According to the Nørskov classical scaling law [16] when x increases on an adsorbate as XH_x, connected to a transition metal surface through the X atom (X can be for instance C, N or O), the interaction energy with surface will decrease.

We will discuss here how such scaling rules vary with adsorption site. We extend the investigation of scaling rule behavior from the late transition metals, as is usually done, to the early transition metals that have so far been much less investigated.

We will see that sometimes exceptions from such valence counting rules are found. For atop adsorbed species the relative stabilities of C versus CH are found to depend on the position of the Fermi level in the molecular orbital partial density of states of the ad atom-surface bond. For these adsorbates classical scaling rule behavior is found only when the Fermi level is located in the antibonding transition metal –adsorbate molecular orbital partial density of states. This is typically the case for the late transition metals but as we have seen in section III not for the early transition metals. Also for the single transition metal atom molecules differences in relative bond energies between M-C and M-CH are found when early and late transition atom molecules are compared.

However, as an important difference between atop and high coordination adsorption is found, since also on the early transition metals surfaces the bond energy of the M-C bond remains stronger than that of the M-CH bond when the adsorbate is at a high coordination site.

As we did in section II we will compare bond energy trends of single transition atom molecules with those of adsorbates to surfaces. Between the molecular bond strengths and interaction energies with the surfaces we will discover a remarkable coincidence in change of scaling law when number of transition metal valence electrons changes.

First scaling rule behavior in transition metal molecules will be discussed, to be followed later with a comparison of scaling rule behavior on surfaces.

In figures 14 and 15 the trends in bond energies of the CH_x and NH_x containing transition metal molecules are compared. An early paper by Carter and Goddard III[63] compared bond energies for selected single transition metal cation molecules with CH_2 and CH, that also demonstrated the stronger bond interaction energies with the latter. An important paper by Siegbahn et.al.[64] made a comparison of the interaction energies of CH_3 and H along a row of the periodic system. Our calculations, over a wider range of x values (x=0-3) for the CH_x and NH_x bonds of the molecular fragments, agree with the trends from the previous studies.

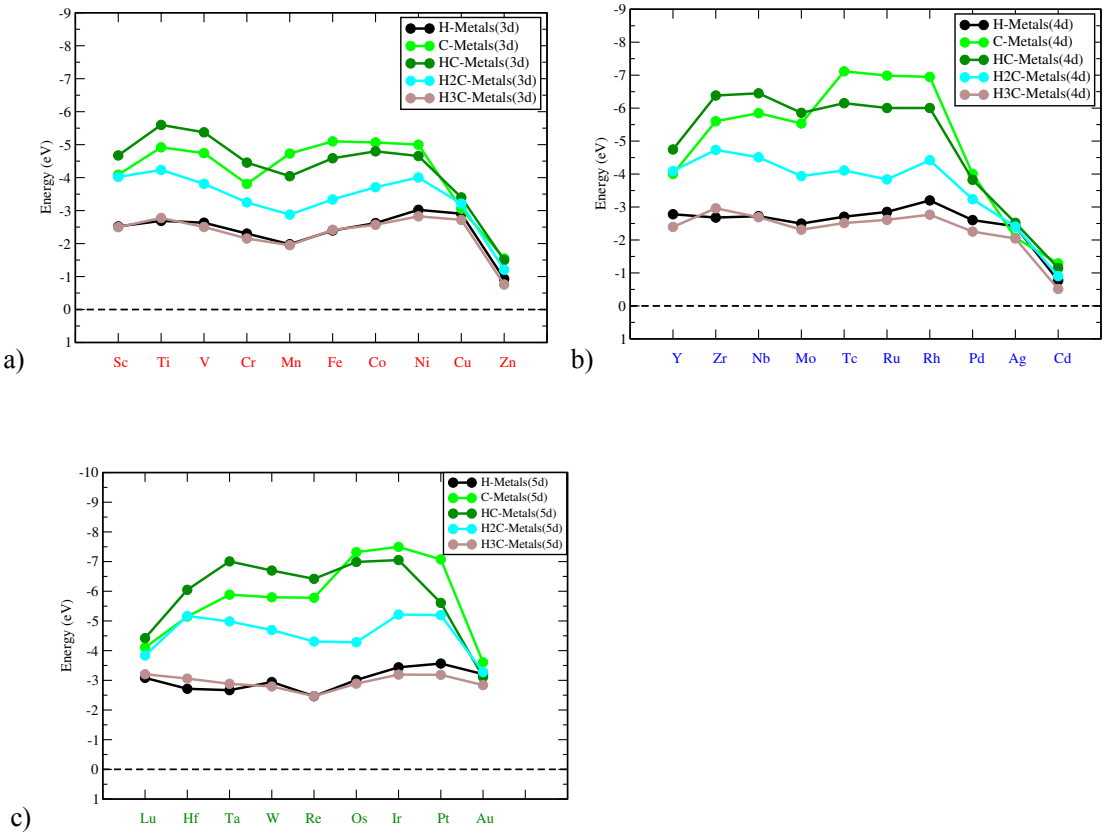

Fig.14 Trends of single transition metal molecular bond energies with CH_x and H as a function of x(x=0-3); a) 3d row transition metal molecules; b) 4^{th} row transition metal molecules; c) 5^{th} row transition metal molecules.

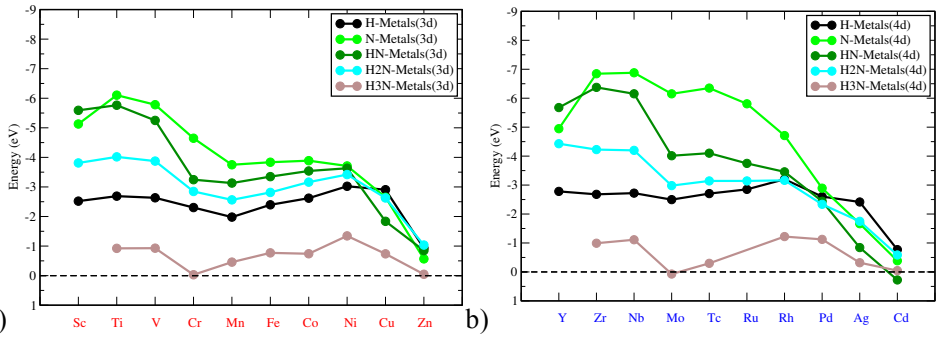

c)

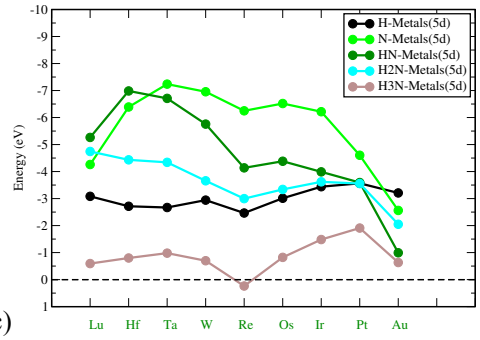

Fig.15 Trends of single transition metal molecular bond energies with NH_x and H as a function of x(x=0-3) a1) 3rd row transition metal molecules; b) 4th row transition metals; c) 5th row transition metal molecules.

In figures 14 and 15 one notes the local minima in the adsorption energies of the molecules when transition metal is varied along a row of the periodic system. As we discussed previously in section II this is due to the varying magnetic stabilization of the reference transition metal atoms in high spin states.

For the late transition metals the classical scaling rule behavior is observed. Bond energies are most strong for the M-C and M-N bonds and they decrease with increasing value of x in CH_x or NH_x. However some of the bond energy curves are seen to cross.

In figures 14 the bond energies of MCH cross the bond energies of MC and in figures 15 not only the curves of MN and MNH cross but even those of MN and MNH_2.

Based on valence bond theory one expects the M-C and M-CH to differ only through one σ bond, the two π bonds remaining constant. Between M-CH and $M-CH_2$ the chemical bond loses a π bond, between $M-CH_2$ and $M-CH_3$ there is also the loss of an additional π bond. CH_3 only interacts through a σ symmetric molecular orbital bond. Therefore its bond energy trend is very similar to that of H. These bonding changes are very similar for the respective $M-NH_x$ molecules.

In the next paragraphs we will limit ourselves to a detailed discussion of the electronic reason for the bond energy crossing of C and CH. The electronic reasons for the bond energy crossing of the NH_x containing molecules are analogous.

From figure 16 we notice that the crossing between M-C and M-CH is present also when the non-spin polarized metal atom is taken as reference. Moreover, the crossing occurs in the same point. Comparing the bond energy maxima of M-C, M-CH and M-O from fig.16 we notice a shift to the left in their position as we go from C to CH and O.

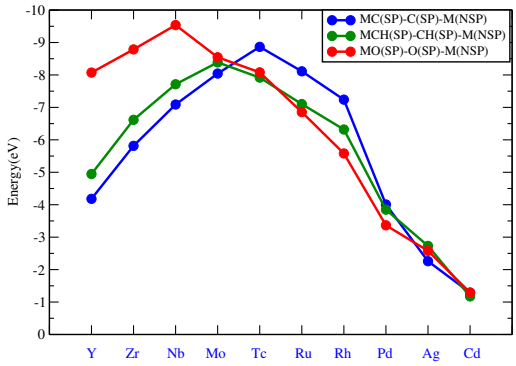

Fig.16 Comparison of the bond energies of CH, C and O on the 4th row transition metals that are referenced to the non-spin polarized transition metal atoms

An elementary explanation for the bond maxima shift and relative bond energy switch can be given based on a united atom model. The united atom view of CH versus C assigns one electron more to the former. The only difference in electronic structure of the M-CH and M-C bonds is its total electron occupation.

In figure 16 at the left of the bond energies maxima only bonding molecular orbitals are occupied, at the right the antibonding molecular orbitals becomes occupied. The bond energy maxima move to the left the more electrons the (united) atom contributes. Therefore the peak in the M-O bond energies of figure 16 is most to the left.

Since it contains an additional electron, more when antibonding orbitals of M-C become occupied more antibonding orbitals are occupied for M-CH than for M-C. This will weaken the M-C bond in M-CH versus that of M-C. On the other hand when only bonding M-C orbitals are occupied, the bond is stronger for M-CH than M-C because of the higher electron occupation of the bonding orbitals. In the case of N this occurs for a lower transition metal electron count compared to C because N has one electron more. Valence electron count rules, as invoked here, that provide compound stability rules are classical to chemistry[6, 65–68].

A calculation of the Bader charges on C of the MCH versus that of MC shows that the C atom is always more negative for MCH (on Nb the difference is 0.07 e.u, on Rh 0.15 e.u). It agrees with the proposed higher electron affinity of the C atom of MCH.

The schematic comparison of the σ symmetric orbital interactions in the MC and MCH molecule from figure 17 can be used to explain the bond energy crossing of the M-C and M-CH molecule based on their molecular orbital structure. The C_{2s} atomic orbital and C_{2pz} atomic orbital interactions are separately indicated. The C_{2s} atomic orbitals do not participate significantly in the M-C chemical bond.

The formation of the M-CH bond is considered to occur in two steps. In the CH fragment the interaction of the C $2p_z$ atomic orbital with the H 1s atomic orbital will form two bonding and antibonding σ symmetric orbitals respectively. Subsequent interaction with the transition metal d_{z^2} atomic orbital generates three new molecular orbitals. In figure 17 the bonding nature of the respective orbitals is indicated. The molecular orbital energy values are taken as calculated for NbCH.

At the left part of figure 17 the molecular orbital energy values are given as calculated for NbC. The Nb $2p_z$ atomic orbital is considered to interact only with the transition metal d_{z^2} atomic orbital, so now one bonding and antibonding molecular orbital is formed.

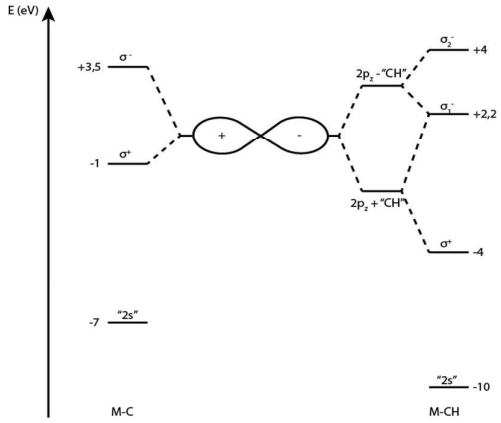

Fig.17 Schematic illustration of the σ symmetric molecules orbitals of M-C and M-CH.

The C_{2pz} -Nb_4 d_{z^2} Nb atomic orbital interaction scheme of NbC compared with that of NbCH.

At low electron occupation the σ+ molecular orbitals are occupied. The bonding σ+ orbital has the lower energy in M-CH. This stabilizes the M-CH bond compared to the M-C molecular bond. Within the rigid band model for the late transition metal molecules the molecular orbital electron occupation increases and nonbonding δ symmetric and the antibonding molecular orbitals become occupied. Because of the low energy of the antibonding σ_1^- orbital in the M-CH chemical bond, this becomes occupied at molecular orbital electron energies where the σ^- orbital in the M-C molecule is not yet occupied. In this molecule initially only nonbonding molecular orbitals become occupied. . Then the stronger M-CH bond energy found for the early transition metal molecules switch to a value smaller than that of the M-C bond. This is the conventional order of bond energies according to the classical scaling rule.

In figures 18 the calculated energy trends for atop and threefold adsorbed C and CH are compared as a function of transition metal along a row of the periodic system. It shows that the inversion in bond energies between C and CH not only is found for the molecules, but also is found for the surfaces. In the case of the surfaces it occurs only for the adsorbate that is atop adsorbed.

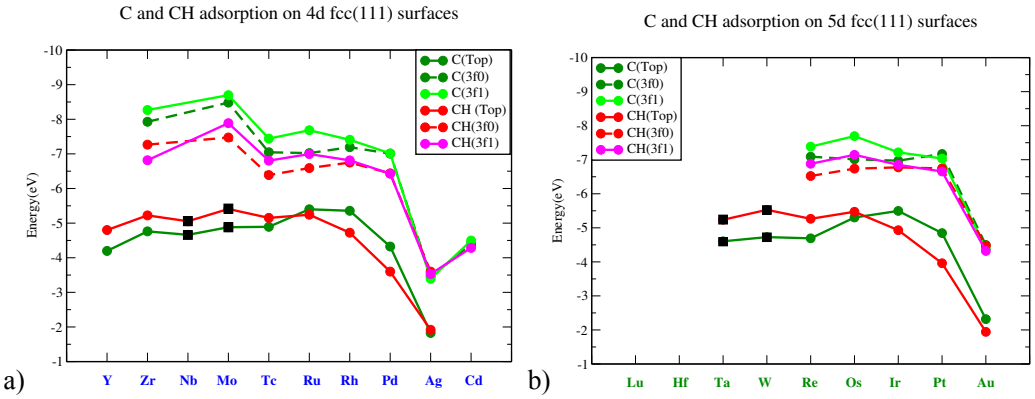

Figures 18. Comparison of trends in bond energies of atop and threefold adsorbed C and CH respectively as a function of transition metal ; a) 4th row transition metals ; b) 5th row transition metals.

The electronic structures of the chemical bonds of atop and threefold adsorbed C and CH on the Rh(111) surface are compared in figures 19. For the atop adsorbed species the COHP of the C $2p_z$-Rh d_{z^2} σ symmetric molecular orbital partial density of states shows a bonding peak at – 7.0 eV for the M-CH chemical bond and around – 4eV a bonding broadened density of states distribution for the M-C bond of the C ad atom . Whereas in this energy interval only bonding molecular orbital partial density of states is occupied for the M-C bond of the C ad atom, antibonding molecular orbital partial density of states is also occupied for the CH ad atom.. There is essentially no change in electron density of the π symmetric interactions.

The reason of the weaker bond of Rh- CH is the additional occupation of antibonding σ symmetric molecular orbital partial density of states, whereas for Rh- C only bonding molecular orbital partial density of states is occupied.

The bond energy trends of figure 18 can be explained within the rigid band model. .A decrease in valence electron occupation will increase the interaction energy of CH, but decrease the bond energy with C. In the case of M-CH antibonding molecular orbital partial density of states depletes, but for M-C bonding molecular orbital density of states depletes. It ultimately results in the inversion of relative bond energies of CH and C that occurs for Tc (a decrease with one valence electron shifts the Fermi level 1 eV downwards)The bond energy crossing occurs when the Fermi level becomes located in the non-bonding M-C molecular orbital partial density of states region of the respected M-C and M-CH chemical bonds.

When threefold coordinated the adsorbate interaction is dominated by the π symmetric molecular orbital interactions. The maximum of the π symmetric bonding molecular orbital partial density of states of the M-C bond of the C ad atom is shifted more downwards in energy than that of M-CH. This is the reason for the stronger M-C bond of the C ad atom.. The change in σ symmetric molecular orbital density of states is comparable to that of the adsorbates that are atop adsorbed. The dominance of the π symmetric bond interactions is the reason of the absence of bond energy crossing for threefold coordinated adsorbates.

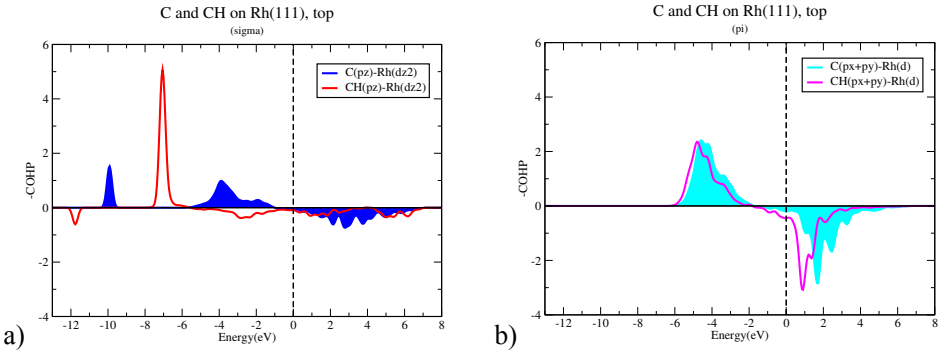

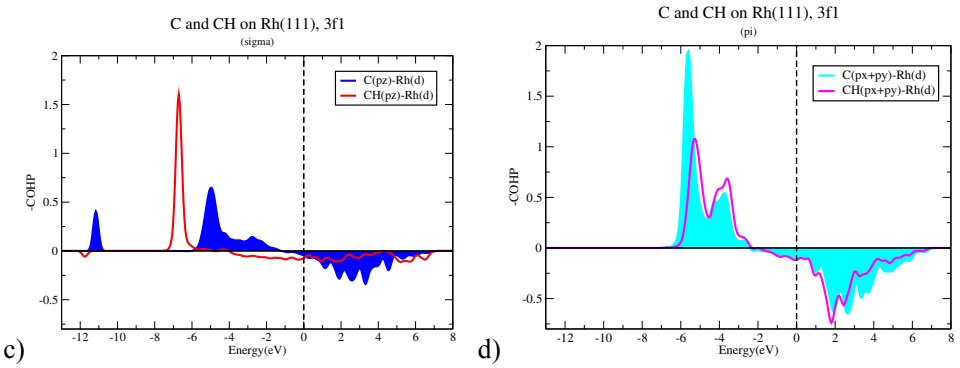

c) d)

Fig.19 a), b) Comparison of the σ and π symmetric -COHP's of atop adsorbed C and CH on the Rh(111) surface; c), d) Comparison of σ and π symmetric -COHP's of three fold adsorbed C and CH. Only the C 2p-Rh d molecular orbital interaction is shown.

The proposition that for atop adsorbed species the relative stability of XH species depends on position of Fermi level in the molecular orbital partial density of states explains why for N versus NH the crossover electron count is at lower transition metal valence electron occupation and also why this cross will not appear for OH. For these adsorbates the Fermi level remains located in the antibonding molecular orbital density of states region at substantially lower values of the transition metal electron occupation than for CH.

VI. Conclusion and discussion

In this paper we have studied the bond energies and electronic structures of the chemical bonds of adsorbates on different surface sites of the early and late transition metals. Bond energy trends of ad atoms have been compared with those of corresponding single transition metal atom molecules. For atop adsorbed species the bond energy trends are approximately similar to those of the transition metal molecules. For threefold adsorbed adsorbates the bond energy trends can be quite different.

The different types of adsorption energy trends one can distinguish are summarized in fig. 20.

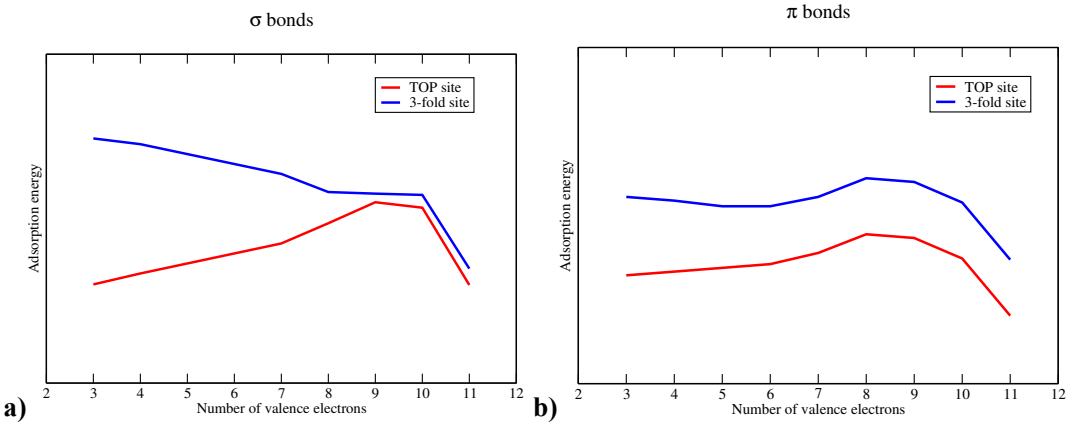

a) b)

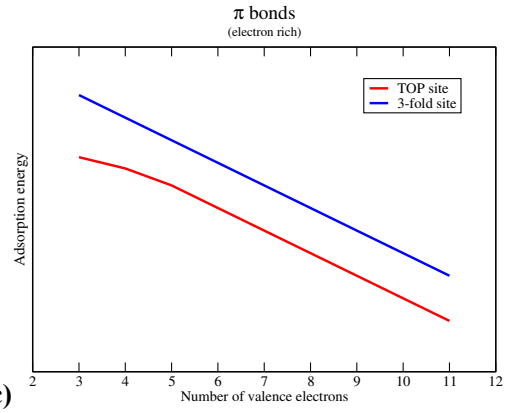

c)

Figure 20. Schematic illustration of the different trends in adsorption energies as a function of adsorption site that illustrate their different dependence as a function of dominating orbital interaction. a) σ symmetric molecular orbital interactions; b) and c) π symmetric orbital interactions. The difference between schematic curves b) and c) is the higher electron affinity of the ad atom in the latter case (e.g. C versus O).This is indicated in fig 20 c) as the π symmetric molecular orbital interaction of an electron rich ad atom.

Figure 20 illustrates for chemical bonds with σ symmetric molecular orbital interactions , such as the M-H or M-CH_3 chemical bonds, the large difference in bond energy trend of the atop and threefold adsorbed adsorbates. Figures 20 also show that when π symmetric orbital interactions dominate chemical bonding trends between atop and threefold adsorbed adsorbates are more parallel. Π symmetric orbital interactions contribute to the M-C and M-O chemical bonds.

This difference in behavior of σ symmetric versus π symmetric orbital interactions has an interesting consequence for scaling rule behavior of the relative bond energies of C and CH.

For the late transition metals when C and CH are adsorbed atop of a surface atom or are part of a single transition metal molecule the bond energies of CH are less than that of C. This is expected based on the classical Nørskov scaling rule [15]. However, for the early transition metals the relative bond energy values interchange and CH interacts more strongly with the transition metal atom than the C atom. When C and CH are threefold adsorbed no such change of the classical scaling rule is found. In section V we have shown that the difference in trend behavior of the chemical bonds of threefold compared to atop adsorbed C and CH relates to the dominance of the π symmetric orbital interaction. When atop adsorbed the σ symmetric interaction dominates and the bond energy of C is only stronger than that of CH as long as the position of the Fermi level is in the antibonding molecular orbital partial density of states.

The larger difference in bond energies of the threefold and atop adsorbed adsorbate is found for the early transition metals that have a low valence electron occupation, only bonding molecular orbital partial density of states being occupied. When the ad atom bond energy is corrected for the embedding energy cost the adsorption energy is nearly proportional to the square root of the number of transition metal atoms that coordinate with adsorbate. According to elementary tight binding theory this is the ratio predicted for chemical bonds of adsorbates with different surface atom coordination number that have only their bonding molecular orbital partial density of states occupied by electrons [6,7,53].

The difference in bond energies of threefold and atop adsorbed adsorbates tends to decrease for the late transition metals. This is due to the increasing contribution of the Pauli repulsive energy contribution to the chemical bond when antibonding molecular orbital density of states becomes occupied by electrons [42, 53],.

According to the covalent rigid band model, that is discussed in detail in section III, the ad atom bond energy decreases when bonding molecular orbital partial density of states gets a lower electron occupation. This would correspond to a decrease in bond energy when interaction with transition metal surfaces is compared between the late and early transition metals. As can be seen in figures 20 the trend in bond energies for the early transition metals is often different from this rigid band prediction. This is due to increasing polarity of the chemical bond for the early transition metals because they have a lower work function [23.24].The increase in bond energy is due to the increasing contribution of the ionic interaction energy to the chemical bond. The polarity of the respective chemical bonds is described in detail in section III.

We have discussed in this paper the difference in chemical bonding of adsorbates attached with different coordination to a transition metal surface. A common denominator of the different bonding aspects that we discussed is the increased Pauli repulsion of the adsorbate chemical bonds to the late transition metals compared to that for adsorbates on the early transition metal surface. This Pauli repulsion increases with adsorbate coordination and is the main reason for the decreased difference in adsorption energies on different sites for the late transition metals. Whereas we did not discuss this, it is the reason that the activation of σ chemical bonds, as for example in methane, occurs preferentially over an atop site[5, 69–71]

When the adsorption energies of atop adsorbed species are compared with the bond energies of corresponding molecules, the adsorbate chemical bonds are always smaller. The difference between adsorbate energies and molecular bond strengths are relevant, because of the increasing interest in single metal atom catalysis [43–45]. This can be illustrated for reactions that activate hydrogen as for instance the electrochemical Hydrogen Evolution Reaction (HER) that reduces protons to H2. The Pt electrode is one of the best electro catalysts for this reaction, since the recombination energy of two adsorbed H atoms is close to the bond energy of H_2. For this reaction the bond energy of H to the transition metal atom or surface can be considered a reactivity performance indicator [72]. Fig. 21 illustrates that the MH bond strengths of the Cr, Fe and Ag transition metal MH or cis MH_2 molecules, are comparable to the bond strength of the H atom adsorbed to the Pt surface. This implies that single atom catalysts are potential non-noble metal catalyst alternatives to Pt.

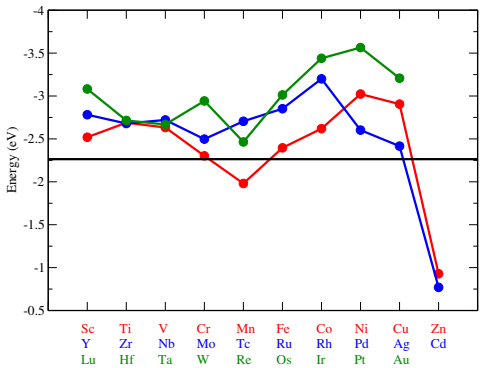

Fig.21 The bond energy of H of the transition metal hydrides. The M-H bond energies of the MH and cis MH_2 molecules are similar. The crossing points with the black line denote the elements of equivalence of H_2 bond energy with twice the MH bond energies.

VII. Computational details and methods

First principle total energy calculations were done using the gradient corrected (PBE) density functional theory as implemented in the Vienna *ab initio* simulation package (VASP) [29–32] in order to identify the stable structural configurations and their respective energies. The electronic wave functions have been expanded into plane waves up to an energy cut-off of 400 eV. A projected-augmented-wave scheme has been used in order to describe the interactions between the valence electrons and the nuclei (ions). The minimum energy configurations for the considered structures have been considered to be reach when the forces on each atom of the systems were less than 0.02 eV/Å. A number of 17x17x17 k-points has been used for the bulk simulations in order to span the Brillouin zone. For the surface calculations (3x3x1 periodicity) this number was lowered to 5x5x1 k-points. Due to the large size of the unit cell considered, only 1 k-point – the Gamma point - was necessary for the molecular systems. High accuracy settings have been enforced throughout.

All the structures of molecules and surfaces studied in this paper have been geometry optimized, except when mentioned otherwise. The surface transition metal atom slabs have 7 layers and their first two layers have been allowed to relax.

The electronic analysis for our systems has been performed through the use of the crystal orbital Hamiltonian population (COHP) and density of states (DOS) functions. Both quantities were computed with the help of the Lobster code [25, 27, 73].

The partial density of states (PDOS) measures as a function of electron energy the probability of an electron to be located in a particular atomic orbital. The mathematical expression for the PDOS in atomic orbital *i* is:

$$\mathrm{PDOS_i}\left(\mathrm{E}\right) = \sum_{\mathrm{n}} \varphi_{\mathrm{i}} | \psi_{\mathrm{n}} \delta\left(\mathrm{E} - \mathrm{E_n}\right) \psi_{\mathrm{n}} | \varphi_{\mathrm{i}} \qquad \text{(Eq. 1a)}$$

$$= \sum_{\mathrm{n}} \left| c_i^n \right|^2 \delta\left(\mathrm{E} - \mathrm{E_n}\right) \qquad \text{(Eq. 1b)}$$

The bracket notation $\langle \phi_{\mathrm{i}} | \phi_{\mathrm{n}} \rangle$ means that the integral over the volume has to be taken. The coefficients c_i^n and the atomic orbitals ϕ_{i} are part of the molecular orbital ϕ_{n} defined by:

$$\psi_n = \sum_i c_i^n \varphi_i \qquad \text{(Eq. 2)}$$

E_n represents the Kohn-Sham orbital energies.

Eq. 1b is only strictly valid when an orthogonal atomic basis set $|\varphi_i\rangle$ is used, so that $S_{ij}=0$ when $i \neq j$;

$$S_{ij} = \langle \phi_i | \phi_j \rangle \qquad \text{(Eq. 3)}$$

The crystal orbital Hamiltonian population density (COHP) measures the magnitude and sign of the bond order energy overlap between atomic orbitals located on different atoms. This enables the determination of the bonding versus the antibonding nature of orbital fragments. It is also a measure of the interaction strength between two atomic orbitals.

$$-\mathrm{COHP_{ij}}(\mathrm{E}) = H_{ij} \cdot P_{ij}(E) \qquad \text{(Eq. 4a)}$$

$$= H_{ij} \sum_{\mathrm{n}} c_i^n c_j^n \delta(\mathrm{E} - \mathrm{E_n}) \qquad \text{(Eq. 4b)}$$

$$\mathrm{ICOHP} = \int_{-\infty}^{E_F} dE \sum_{i,j} COHP_{ij}(E) \qquad \text{(Eq. 5a)}$$

$$= \frac{1}{2} \sum_{N_i}^{occ} N_i E_i \qquad \text{(Eq. 5b)}$$

N_i is the electron occupation of molecular orbital ψ_i in Eq. 5. The Eq. 5b is valid for non-spin polarized systems.

The integrated ICOHP value can be considered a measure of the bond strength. It is not an exact expression for the bond energy, but a good approximation as long as the repulsive energy of the nuclei cancels against the double counted electrostatic interactions [26].

-ICOHP is maximum for a covalent bond when all bonding orbitals are occupied by electrons and none of the antibonding orbitals. For an ionic system, the smaller the relative value of -ICOHP the more ionic is the bond.

In order to calculate the COHP and the PDOS, orthogonalized basis functions must be used, for example those developed by using the Löwdin orthogonalization method [74].

In order to calculate the Bader charges and topological electron density properties the weight method of Yu and Trinkle has been used[33–37]

References

1. Nørskov, J. K., Studt, F., Abild-Pedersen, F., and Bligaard, T. (2014). Fundamental Concepts in Heterogeneous Catalysis (Wiley).

2. Wang, S., Petzold, V., Tripkovic, V., Kleis, J., Howalt, J. G., Skúlason, E., Fernández, E. M., Hvolbæk, B., Jones, G., Toftelund, A., et al. (2011). Universal transition state scaling relations for (de)hydrogenation over transition metals. Phys. Chem. Chem. Phys. *13*, 20760. Available at: http://xlink.rsc.org/?DOI=c1cp20547a.

3. Calle-Vallejo, F., Inoglu, N. G., Su, H.-Y., Martinez, J. I., Man, I. C., Koper, M. T. M., Kitchin, J., and Rossmeisl, J. (2013). Number of outer electrons as descriptor for adsorption processes on transition metals and their oxides. Chem. Sci. *4*, 1245.

4. Calle-Vallejo, F., Martínez, J. I., García-Lastra, J. M., Rossmeisl, J., and Koper, M. T. M. (2012). Physical and Chemical Nature of the Scaling Relations between Adsorption Energies of Atoms on Metal Surfaces. Phys. Rev. Lett. *108*, 116103.

5. Chin, Y.-H. C., Buda, C., Neurock, M., and Iglesia, E. (2013). Consequences of metal-oxide interconversion for C-H bond activation during CH4 reactions on Pd catalysts. J. Am. Chem. Soc. *135*, 15425–15442.

6. van Santen, R. A., and Filot, I. A. W. (2013). Quantum Chemistry of Transition Metal Surface Bonding and Reactivity. In The Chemical Bond, G. Frenking and S. Shaik, eds. (Wiley-VCH), pp. 269–335.

7. van Santen, R. A., and Neurock, M. (2006). Molecular Heterogenous Catalysis (Wiley-VCH).

8. Gross, A. (2009). Theoretical Surface Science (Berlin: Springer Verlag).

9. Miller, D. J., Öberg, H., Kaya, S., Sanchez Casalongue, H., Friebel, D., Anniyev, T., Ogasawara, H., Bluhm, H., Pettersson, L. G. M., and Nilsson, a. (2011). Oxidation of Pt(111) under Near-Ambient Conditions. Phys. Rev. Lett. *107*, 195502.

10. Nilsson, A., Pettersson, L. G. M., and Nørskov, J. K. (2008). Chemical Bonding at Surfaces and Interfaces. In Chemical Bonding at Surfaces and Interfaces (Elsevier), pp. 255–322.

11. Föhlisch, A., Nyberg, M., Bennich, P., Triguero, L., Hasselström, J., Karis, O., Pettersson, L. G. M., and Nilsson, A. (2000). The bonding of CO to metal surfaces. J. Chem. Phys. *112*, 1946. Available at: http://scitation.aip.org/content/aip/journal/jcp/112/4/10.1063/1.480773.

12. Mavrikakis.M, Hammer.B, Nørskov ,J.K.(1998), Effect of strain on the reactivity of metal surfaces, Phys. Rev.Lett.*55*,2618

13. Pettersson, L. G. M., and Nilsson, A. (2013). A Molecular Perspective on the d-Band Model: Synergy Between Experiment and Theory. Top. Catal. *57*, 2–13. Available at: http://dx.doi.org/10.1007/s11244-013-0157-4.

14. Schimka, L., Harl, J., Stroppa, A., Grüneis, A., Marsman, M., Mittendorfer, F., and Kresse, G. (2010). Accurate surface and adsorption energies from many-body perturbation theory. Nat. Mater. *9*, 741–744. Available at: http://www.nature.com/doifinder/10.1038/nmat2806.

15. Nørskov, J. K., Abild-Pedersen, F., Studt, F., and Bligaard, T. (2011). Density functional theory in surface chemistry and catalysis. Proc. Natl. Acad. Sci. U. S. A. *108*, 937–943. Available at: http://www.pubmedcentral.nih.gov/articlerender.fcgi?artid=3024687{&}tool=pmcentrez{&}rendertype=abstract.

16. Abild-Pedersen, F., Studt, F., Rossmeisl, J., Munter, T. R., Moses, P. G., Skúlason, E., Bligaard, T., Nørskov, J. K., and Greely, J. (2007). Scaling Properties of Adsorption Energies for Hydrogen-Containing Molecules on Transition-Metal Surfaces. Phys. Rev. Lett. *99*, 16105–16109.

17. Hammer, B., and Nørskov, J. K. (2000). Impact of Surface Science on Catalysis. Adv. Catal. *45*, 71–129.

18. Shustorovich, E. (1986). Chemisorption phenomena: Analytic modeling based on perturbation theory and bond-order conservation. Surf. Sci. Rep. *6*, 1–63. Available at: http://linkinghub.elsevier.com/retrieve/pii/0167572986900038.

19. Calle-Vallejo, F., Loffreda, D., Koper, M. T. M., and Sautet, P. (2015). Introducing structural sensitivity into adsorption – energy scaling relations by means of coordination numbers. Nat. Chem. Available at: http://dx.doi.org/10.1038/nchem.2226.

20. van Santen, R. A., Neurock, M., and Shetty, S. (2010). Reactivity Theory of Transition-Metal Surfaces: A Br{ø}nsted−Evans−Polanyi Linear Activation Energy−Free-Energy Analysis. Chem. Rev. *110*, 2005–2018.

21. Nørskov, J. K., Bligaard, T., Rossmeisl, J., and Christensen, C. H. (2009). Towards the computational design of solid catalysts. Nat. Chem. *1*, 37–46. Available at: http://www.nature.com/doifinder/10.1038/nchem.121.

22. Michaelides, A., Liu, Z.-P., Zhang, C. J., Alavi, A., King, D. A., and Hu, P. (2003). Identification of general linear relationships between activation energies and enthalpy changes for dissociation reactions at surfaces. J. Am. Chem. Soc. *125*, 3704–3705. Available at: http://www.ncbi.nlm.nih.gov/pubmed/12656593.

23. Hoffmann, R. (1988). Solids and Surfaces (Weinheim: VCH).

24. Hoffmann, R. (1988). A chemical and theoretical way to look at bonding on surfaces. Rev. Mod. Phys. *60*, 601–628. Available at: http://link.aps.org/doi/10.1103/RevModPhys.60.601.

25. Deringer, V. L., Tchougréeff, A. L., and Dronskowski, R. (2011). Crystal orbital Hamilton population (COHP) analysis as projected from plane-wave basis sets. J. Phys. Chem. A *115*, 5461–5466.

26. Landrum, G. A., and Dronskowski, R. (2000). The Orbital Origins of Magnetism: From Atoms to Molecules to Ferromagnetic Alloys. Angew. Chemie Int. Ed. *39*, 1560–1585. Available at: http://doi.wiley.com/10.1002/{%}28SICI{%}291521-3773{%}2820000502{%}2939{%}3A9{%}3C1560{%}3A{%}3AAID-ANIE1560{%}3E3.0.CO{%}3B2-T.

27. Dronskowski, R., and Bloechl, P. E. (1993). Crystal orbital Hamilton populations (COHP): energy-resolved visualization of chemical bonding in solids based on density-functional calculations. J. Phys. Chem. *97*, 8617–8624. Available at: http://pubs.acs.org/doi/abs/10.1021/j100135a014.

28. Van den Hoek, P. J., Baerends, E. J., and Van Santen, R. A. (1989). Ethylene epoxidation on silver(110): the role of subsurface oxygen. J. Phys. Chem. *93*, 6469–6475. Available at: http://pubs.acs.org/doi/abs/10.1021/j100354a038.

29. Kresse, G., and Furthmüller, J. (1996). Efficiency of ab-initio total energy calculations for metals and semiconductors using a plane-wave basis set. Comput. Mater. Sci. *6*, 15–50. Available at: http://linkinghub.elsevier.com/retrieve/pii/0927025696000080.

30. Kresse, G., and Hafner, J. (1993). Ab initio molecular dynamics for liquid metals. Phys. Rev.

B *47*, 558–561. Available at: http://link.aps.org/doi/10.1103/PhysRevB.47.558.

31. Kresse, G., and Hafner, J. (1994). Ab initio molecular-dynamics simulation of the liquid-metal–amorphous-semiconductor transition in germanium. Phys. Rev. B *49*, 14251–14269. Available at: http://link.aps.org/doi/10.1103/PhysRevB.49.14251.

32. Kresse, G., and Furthmüller, J. (1996). Efficient iterative schemes for ab initio total-energy calculations using a plane-wave basis set. Phys. Rev. B *54*, 11169–11186. Available at: http://link.aps.org/doi/10.1103/PhysRevB.54.11169.

33. Tang, W., Sanville, E., and Henkelman, G. (2009). A grid-based Bader analysis algorithm without lattice bias. J. Phys. Condens. Matter *21*, 084204. Available at: http://stacks.iop.org/0953-8984/21/i=8/a=084204?key=crossref.84a8e56b7ca1da94922dada58295eda5.

34. Sanville, E., Kenny, S. D., Smith, R., and Henkelman, G. (2007). Improved grid-based algorithm for Bader charge allocation. J. Comput. Chem. *28*, 899–908. Available at: http://doi.wiley.com/10.1002/jcc.20575.

35. Henkelman, G., Arnaldsson, A., and Jónsson, H. (2006). A fast and robust algorithm for Bader decomposition of charge density. Comput. Mater. Sci. *36*, 354–360. Available at: http://linkinghub.elsevier.com/retrieve/pii/S0927025605001849.

36. Yu, M., and Trinkle, D. R. (2011). Accurate and efficient algorithm for Bader charge integration. J. Chem. Phys. *134*, 064111. Available at: http://scitation.aip.org/content/aip/journal/jcp/134/6/10.1063/1.3553716.

37. Vega, D., and Almeida, D. (2014). AIM-UC: An application for QTAIM analysis. J. Comput. Methods Sci. Eng. *14*, 131–136.

38. Hopffgarten, M. von, and Frenking, G. (2012). Energy decomposition analysis. Wiley Interdiscip. Rev. Comput. Mol. Sci. *2*, 43–62. Available at: http://doi.wiley.com/10.1002/wcms.71.

39. Ziegler, T., and Rauk, A. (1977). On the calculation of bonding energies by the Hartree Fock Slater method. Theor. Chim. Acta *46*, 1–10. Available at: http://link.springer.com/10.1007/BF02401406.

40. Delley, B., Ellis, D. E., Freeman, A. J., Baerends, E. J., and Post, D. (1983). Binding energy and electronic structure of small copper particles. Phys. Rev. B *27*, 2132–2144. Available at: http://link.aps.org/doi/10.1103/PhysRevB.27.2132.

41. E.J.Baerends (1986). Quantum Chemistry: The Challenge of Transition Metals and Coordination Chemistry A. Veillard, ed. (Dordrecht: Springer Netherlands) Available at: http://link.springer.com/10.1007/978-94-009-4656-9.

42. van Santen, R. A., and Baerends, E. J. (1991). Orbital interactions and chemical reactivity of metal particles and surfaces. In Theoretical models of chemical bonding, Z. B. Maksic, ed. (Springer Berlin Heidelberg), pp. 323–389.

43. Sun, S., Zhang, G., Gauquelin, N., Chen, N., Zhou, J., Yang, S., Chen, W., Meng, X., Geng, D., Banis, M. N., et al. (2013). Single-atom Catalysis Using Pt/Graphene Achieved through Atomic Layer Deposition. Sci. Rep. *3*. Available at: http://www.nature.com/articles/srep01775.

44. Yang, X.-F., Wang, A., Qiao, B., Li, J., Liu, J., and Zhang, T. (2013). Single-Atom Catalysts: A New Frontier in Heterogeneous Catalysis. Acc. Chem. Res. *46*, 1740–1748. Available at: http://pubs.acs.org/doi/abs/10.1021/ar300361m.

45. Flytzani-Stephanopoulos, M. (2014). Gold Atoms Stabilized on Various Supports Catalyze the Water–Gas Shift Reaction. Acc. Chem. Res. *47*, 783–792. Available at: http://pubs.acs.org/doi/abs/10.1021/ar4001845.

46. Wang, X., and Andrews, L. (2003). Chromium Hydrides and Dihydrogen Complexes in Solid Neon, Argon, and Hydrogen: Matrix Infrared Spectra and Quantum Chemical Calculations. J. Phys. Chem. A *107*, 570–578. Available at: http://pubs.acs.org/doi/abs/10.1021/jp026930h.

47. Chen, Y.-M., Clemmer, D. E., and Armentrout, P. B. (1993). Gas-phase thermochemistry of VH and CrH. J. Chem. Phys. *98*, 4929. Available at: http://scitation.aip.org/content/aip/journal/jcp/98/6/10.1063/1.464948.

48. Siegbahn, P. E. M., Blomberg, M. R. A., and Bauschlicher, C. W. (1984). The dissociation of H2 on the Ni(100) surface. J. Chem. Phys. *81*, 2103. Available at: http://scitation.aip.org/content/aip/journal/jcp/81/4/10.1063/1.447834.

49. Triguero, L., Pettersson, L. G. M., Minaev, B., and Ågren, H. (1998). Spin uncoupling in surface chemisorption of unsaturated hydrocarbons. J. Chem. Phys. *108*, 1193. Available at: http://scitation.aip.org/content/aip/journal/jcp/108/3/10.1063/1.475481.

50. Lejaeghere, K., Van Speybroeck, V., Van Oost, G., and Cottenier, S. (2014). Error Estimates for Solid-State Density-Functional Theory Predictions: An Overview by Means of the Ground-State Elemental Crystals. Crit. Rev. Solid State Mater. Sci. *39*, 1–24. Available at: http://www.tandfonline.com/doi/abs/10.1080/10408436.2013.772503.

51. Kelly, M. J. (1974). Some Comments on the Valence Bands of Model Amorphous Semiconductor Structures. In Tetrahedrally Bonded Amorphous Semiconductors: International Conference (ASCE), pp. 174–176.

52. Zonnevylle, M. C., Hoffmann, R., van den Hoek, P. J., and van Santen, R. A. (1989). Covalent effects in molecule-surface charge exchange: O2 on Ag(111). Surf. Sci. *223*, 233–257. Available at: http://linkinghub.elsevier.com/retrieve/pii/003960288990736X.

53. van Santen, R. A. (1991). Theoretical Heterogeneous Catalysis 1st ed. (World Scientific).

54. Bader, R. F. W. (1994). Atoms in Molecules; A quantum theory.

55. Matta, C. F., and Boyd, R. J. (2007). Introduction to the quantum theory of atoms in molecules. In The Quantum Theory of Atoms in Molecules, C. F. Matta and R. J. Boyd, eds. (Wiley VCH), pp. 1–34.

56. Walch, S. P., and Bauschlicher, C. W. (1985). Comparison of Ab Initio Quantum Chemistry with Experiment for Small Molecules: The State of the Art Proceedings of a Symposium Held at Philadelphia, Pennsylvania, 27--29 August, 1984. In, R. J. Bartlett, ed. (Dordrecht: Springer Netherlands), pp. 17–51. Available at: http://dx.doi.org/10.1007/978-94-009-5474-8_2.

57. Bagus, P. S., and Björkman, C. (1981). Electronic structure of transition-metal hydrides: NiH and PdH. Phys. Rev. A *23*, 461–472. Available at: http://link.aps.org/doi/10.1103/PhysRevA.23.461.

58. Koseki, S., Ishihara, Y., Umeda, H., Fedorov, D. G., and Gordon, M. S. (2002). Dissociation Potential Curves of Low-Lying States in Transition Metal Hydrides. I. Hydrides of Group 4. J. Phys. Chem. A *106*, 785–794. Available at: http://pubs.acs.org/doi/abs/10.1021/jp012644e.

59. Andrews, L. (2004). Matrix infrared spectra and density functional calculations of transition metal hydrides and dihydrogen complexes. Chem. Soc. Rev. *33*, 123. Available at: http://xlink.rsc.org/?DOI=b210547k.

60. Langhoff, S. R., Bauschlicher, C. W., Rendell, A. P., and Komornicki, A. (1990). Theoretical study of the radiative lifetime of the A 1∏u state of C2. J. Chem. Phys. *92*, 6599. Available at: http://scitation.aip.org/content/aip/journal/jcp/92/11/10.1063/1.458297.

61. Greenwood, N. N. (1968). Ionic Crystals, Lattice Defects and Nonstoichiometry (London: Butterworth and Co.).

62. Carter, E. A., and Koel, B. E. (1990). A method for estimating surface reaction energetics: Application to the mechanism of ethylene decomposition on Pt(111). Surf. Sci. *226*, 339–357. Available at: http://linkinghub.elsevier.com/retrieve/pii/003960289090498W.

63. Carter, E. A., and Goddard, W. A. (1988). Relationships between bond energies in coordinatively unsaturated and coordinatively saturated transition-metal complexes: a quantitative guide for single, double, and triple bonds. J. Phys. Chem. *92*, 5679–5683. Available at: http://pubs.acs.org/doi/abs/10.1021/j100331a026.

64. Wittborn, A. M. C., Costas, M., Blomberg, M. R. A., and Siegbahn, P. E. M. (1997). The C–H activation reaction of methane for all transition metal atoms from the three transition rows. J. Chem. Phys. *107*, 4318. Available at: http://scitation.aip.org/content/aip/journal/jcp/107/11/10.1063/1.474772.

65. Hoffmann, R., and Woodward, R. B. (1967). The Conservation of Orbital Symmetry.

66. Albright, T. A., Burdett, J. K., and Whangbo, M.-H. (2013). Orbital Interactions in Chemistry (Wiley).

67. Mingos, D. M. P. (1998). Essential Trends in Inorganic Chemistry (Oxford University Press).

68. Tolman, C. A. (1972). The 16 and 18 electron rule in organometallic chemistry and homogeneous catalysis. Chem. Soc. Rev. *1*, 337. Available at: http://xlink.rsc.org/?DOI=cs9720100337.

69. Qi, Q., Wang, X., Chen, L., and Li, B. (2013). Methane dissociation on Pt(111), Ir(111) and PtIr(111) surface: A density functional theory study. Appl. Surf. Sci. *284*, 784–791. Available at: http://linkinghub.elsevier.com/retrieve/pii/S0169433213014864.

70. Wang, B., Song, L., and Zhang, R. (2012). The dehydrogenation of CH4 on Rh(111), Rh(110) and Rh(100) surfaces: A density functional theory study. Appl. Surf. Sci. *258*, 3714–3722. Available at: http://linkinghub.elsevier.com/retrieve/pii/S0169433211019039.

71. Chin, Y.-H. C., Buda, C., Neurock, M., and Iglesia, E. (2011). Reactivity of Chemisorbed Oxygen Atoms and Their Catalytic Consequences during CH4–O2 Catalysis on Supported Pt Clusters. J. Am. Chem. Soc. *133*, 15958–15978. Available at: http://www.ncbi.nlm.nih.gov/pubmed/21919447.

72. Nørskov, J. K., Bligaard, T., Logadottir, A., Kitchin, J. R., Chen, J. G., Pandelov, S., and Stimming, U. (2005). Trends in the Exchange Current for Hydrogen Evolution. J. Electrochem. Soc. *152*, J23. Available at: http://jes.ecsdl.org/cgi/doi/10.1149/1.1856988.

73. Maintz, S., Deringer, V. L., Tchougréeff, A. L., and Dronskowski, R. (2013). Analytic projection from plane-wave and PAW wavefunctions and application to chemical-bonding analysis in solids. J. Comput. Chem. *34*, 2557–2567.

74. Löwdin, P.-O. (1950). On the Non-Orthogonality Problem Connected with the Use of Atomic Wave Functions in the Theory of Molecules and Crystals. J. Chem. Phys. *18*, 365. Available at: http://scitation.aip.org/content/aip/journal/jcp/18/3/10.1063/1.1747632.